Vision Research 60 (2012) 79–94

Contents lists available at SciVerse ScienceDirect

Vision Research

journal homepage: www.elsevier.com/locate/visres

Temporal dynamics of the Venetian blind effect

Joshua Jay Dobias *, Wm Wren Stine

University of New Hampshire, USA

ARTICLE INFO

Article history:
Received 29 June 2011
Received in revised form 17 February 2012
Available online 7 March 2012

Keywords:
Stereopsis
Irradiation stereoscopy
Venetian blind effect
Contrast disparity
Luminance disparity
Temporal dynamics
Motion-in-depth

ABSTRACT

When square wave gratings are viewed binocularly with lower luminance or contrast in one eye, the individual bars of the grating appear to rotate around a vertical axis (Venetian blind effect). The effect has typically been thought to occur due to retinal disparities that result from irradiation and, therefore, are entirely entoptic. If so, the visual system should process disparities from a luminance or contrast disparity and a geometric disparity at the same rate. Studies of motion-in-depth using geometric disparities have shown that the visual system is unable to process depth cues when those cues are oscillated at frequencies greater than 5 Hz. By changing contrast (experiments one and two) and geometric (experiment three) disparity cues over time, the present study measured the frequency at which both the perception of motion-in-depth and the perception of depth diminish. The perception of motion-in-depth from contrast disparities decreased near 1.1 Hz (experiments one and four) and the perception of depth from contrast disparities decreased near 1.3 Hz (experiments one, two and four); both of which are lower than the frequency where depth from a geometric disparity diminished (near 4.8 Hz in experiment three). The differences between the dynamics of depth from contrast and geometric disparities suggest that the perception arises from separate neural mechanisms.

1. Introduction

Individuals with binocular vision typically use the slight geometric differences between the images on each retina as cues for depth. However, stimuli can appear to rotate around a vertical axis when the image shown to one eye has lower luminance (Cibis & Haber, 1951; Münster, 1941) or lower Michelson contrast[1] (Fiorentini & Maffei, 1971, experiment three; Filley et al., 2011) compared to the image shown to the other eye[2] (Venetian blind effect).

1.1. Venetian blind effect

At least two theories ascribe the Venetian blind effect to the creation of a geometric retinal disparity by the optics of the eye. Cibis and Haber (1951) state that, when there is a decrease in retinal illuminance in one eye, the eye's optics (e.g., Losada, Navarro, & Santamaría, 1993; Westheimer, 2007) cause a shift in the location where the retinal illuminance of the grating bars cross threshold. This shift, in turn, causes the brighter bars to appear physically wider in the eye receiving higher average retinal illuminance than those in the eye viewing the lower average luminance, creating a geometric disparity between the two retinal images (see Howard & Rogers, 1995, p. 310). Ogle (1962) coined the term irradiation stereoscopy for perceived depth that results from pre-retinal optics.

A second theory may be derived from von Helmholtz's (1911/1924, pp. 186–193) suggestion that the eye's imperfect optics (see von Helmholtz, 1911/1924, Fig. 35) followed by the compressive non-linearity of the visual system's response to retinal illuminance would cause the location of an edge to appear shifted toward the less intense side (von Helmholtz, 1911/1924, p. 189). As a result, a square-wave grating viewed binocularly with an average luminance or contrast disparity would appear to have rotated bright bars due to the increased apparent width of those bars in the higher-intensity image relative to that in the lower-intensity image (Filley et al., 2011).

von Békésy (1970) suggested that the apparent rotation of a surface while looking through a neutral density filter is likely a "complicated combination of irradiation and lateral nervous interaction" (p. 347) because the perceived magnitude of rotation of a square-wave grating's darker bars appears to increase when that grating is placed next to a white field. Of course, such effects

* Addresses: Laboratory of Vision Research/Center for Cognitive Science, Rutgers University, Piscataway, NJ 08854-8020, USA (J.J. Dobias), Department of Psychology, Conant Hall, University of New Hampshire, Durham, NH 03824, USA (W.W. Stine).

E-mail addresses: joshua.dobias@gmail.com, jjd242@rci.rutgers.edu (J.J. Dobias), bill.stine@unh.edu (W.W. Stine).

[1] Michelson contrast is defined as the difference between the maximum and minimum luminance values divided by the sum of the maximum and minimum luminance values, or $((L_{max} - L_{min})/(L_{max} + L_{min}))$ (Michelson, 1927).

[2] Blake and Cormack (1979) failed to replicate the results of Fiorentini and Maffei (1971).

0042-6989/$ - see front matter © 2012 Elsevier Ltd. All rights reserved.
http://dx.doi.org/10.1016/j.visres.2012.02.013

may be due to stereo contrast rather than the result of processes associated directly with the Venetian blind effect (Filley et al., 2011).

Filley et al. (2011) tested both irradiation theories using stimuli of moderate contrast. Experiment one showed that subjects reported rotation with gratings of less-than-unity contrast, contradicting the model proposed by Cibis and Haber (1951; Filley et al., 2011, Appendix B) since that model requires the dark portions of the stimulus to be below threshold. Further, the pattern of results did not match the predictions from a model based on irradiation that combined the human point-spread function (Westheimer, 2007, p. 487) with a compressive nonlinearity using the Naka-Rushton equation (Naka & Rushton, 1966, Eq. (1)).

von Helmholtz irradiation predicts that the perceived location of a blurred edge shifts toward the darker region as a function of increasing blur width, or decreasing blur spatial frequency, which has been measured (Bex & Edgar, 1996; Mather & Morgan, 1986; Morgan et al., 1984). Further, threshold retinal disparities and stereo efficiency should decrease with blur width, or decreasing blur spatial frequency, for blurs larger than about 25 min of arc, or spatial frequencies below 2.4 c/deg (Schor & Wood, 1983; Schor, Wood, & Ogawa, 1984). Hence, an irradiation model with the compressive nonlinearity would predict that Venetian blind induced perceived rotation would increase as a function of blur width up to 25 min of arc, and then decrease for wider widths due to the relatively larger effect of blur width on efficiency than perceived edge movement (Filley et al., 2011). However, the threshold for perceived rotation and the amount of perceived rotation remain constant as a function of increases in blur width, contradicting the irradiation model with a compressive nonlinearity (Filley et al., 2011). Filley et al. developed an intensity-difference model relating the interocular difference in retinal illuminance of the light bars of the grating to the probability of perceiving rotation that did fit the observed data.[3] Further, they suggested that their subjects were operating in the linear range of the compressive nonlinearity.

1.2. Temporal characteristics of stereopsis and motion-in-depth

For local and global stereopsis, the amount of disparity necessary to perceive depth increases as a function of the reduction in stimulus exposure time (White & Odom, 1985). Several studies have shown that the perception of depth decreases as the frequency of the depth changes increases; decreasing at frequencies between 1 and 2 Hz and diminishing completely between 4 and 6 Hz (Beverley & Regan, 1973a, 1973b, 1974a, 1974b; Regan & Beverley, 1973a, 1973b; Richards, 1972).

1.3. Present study: temporal dynamics of the Venetian blind effect

Filley et al. (2011) informally observed that perceived rotation lags the onset of an average luminance disparity when that disparity gradually increases over a brief period. The two irradiation models described above would predict that critical frequencies for the Venetian blind effect should approximate 5 Hz, matching that for a geometric disparity. Further, a simple filter model would predict that the critical frequency for a sine-wave contrast modulation[4] should match that for a square-wave contrast modulation. Our overall goal, then, was to compare the critical frequency of a sine-wave contrast disparity modulation, in experiment one, to the critical frequency of a square-wave contrast modulation, in experiment two, and both of these to that of a geometric disparity modulation, measured in experiment three. Finally, we directly measured one's ability to discriminate perceived rotation induced by sine-wave contrast modulations from those induced by square-wave contrast modulations in experiment four.

2. General methods

2.1. Apparatus

Sitting in a dark room, participants used a bite bar while viewing the stimuli through 3 mm apertures. Stimuli were presented on a LaCie electron19blueIV monitor with a refresh rate of 85 Hz at a distance of 1.58 m. One pixel took up 38 s of visual angle. A Power Mac G4 MDD computer running *Mathematica* 4.2.1.0 generated the animated stimuli and recorded responses.

Luminance measures were taken with a Minolta LS-110 photometer. The maximum and minimum luminance values generated by the monitor were approximately 86 and 2 cd/m^2, respectively. The monitor was gamma corrected. The standard average luminance value for stimulus presentation was set to 29 cd/m^2, and the maximum contrast value was set to 0.65.

Each frame of the animation consisted of two square wave gratings placed side-by-side (Fig. 1a). A baffle was placed vertically between the two gratings. Each grating consisted of four dark bars and three light bars, each of which was 1.6° in height and 0.410° in width (with the exception of experiment three, where the width of bars were manipulated). Each complete grating had a spatial frequency of 1.25 cycles per degree, and was 1.6° in height and 2.8° in width with an overall luminance of 29 cd/m^2 (equal to the luminance of the background), and an overall contrast of 0.325. Above and below each grating, 0.03° lines were placed to aid in the fusion of the two images. The center of each line contained a 0.1° by 0.5° vertical rectangle with the same luminance as each dark bar of the left grating.

2.2. Procedure

Subjects sat in a chair biting on a properly positioned bite bar. A pair of apertures with adjustable diameters were reduced to 3 mm and aligned to the stimuli on the monitor, the room was darkened, and the experimenter exited the room. The subject initiated the start of the experiment and then viewed a blank gray screen with a luminance of 29 cd/m^2 for 5 min. After adaptation, a trial began with the presentation of a stimulus containing only lines for 10 s

[3] It is not at all clear why the visual system would respond to a contrast disparity. A contrast disparity would occur when a vertical surface that exhibits both specular and diffuse reflection is rotated out of the fronto-parallel plane and the source of illumination comes from behind the observer. One might speculate that responding to a contrast disparity with perceived rotation would enable seeing the real rotation at distances that might be too large for a rotation to be perceived using geometric disparity alone. Further, at very high contrasts, the apparent increase in the size of a stimulus with luminance, presumably due to irradiation, can support perceived rotation when there is a luminance disparity (e.g., 50 cd/m^2 presented to one eye and 100 cd/m^2 presented to the other with dark surrounds).

[4] Our definition of a contrast modulation differs from that used by Hetley and Stine (2011) because their monitor generated much higher luminance values than the monitor used for the present experiments. Therefore, for Hetley and Stine, an image with a contrast modulation of 1.0 would have a 100% contrast in the image shown to one eye while a contrast modulation of 1.0 in our studies would have 65% contrast in one eye. The contrast of the image in one eye can be calculated using the equation $con = (avgcon)(1 \pm conmod)$, where *con* is the contrast of the grating in one eye, *avgcon* is the average contrast of the two gratings, and *conmod* is the contrast modulation used for the two gratings. Hetley and Stine (2011) used 5.7 c/deg gratings with angular disparities of 12.2, 24.3, 36.5 or 48.7 s of arc that were canceled using contrast, or luminance, disparities. Interpolating from their data, a Hetley and Stine (2011) modulation of about 0.60 should cancel an edge disparity of 38 s of arc, corresponding to an interocular contrast difference from a contrast modulation of 0.92 for our study. Of course, the interocular ratio of grating contrasts for a Hetley and Stine (2011) modulation 0.60 matched that for a 0.60 modulation in the present study. The range of contrast modulations used in experiments one and two, 0.20–1.00, covers the range needed to cancel the presented disparity.

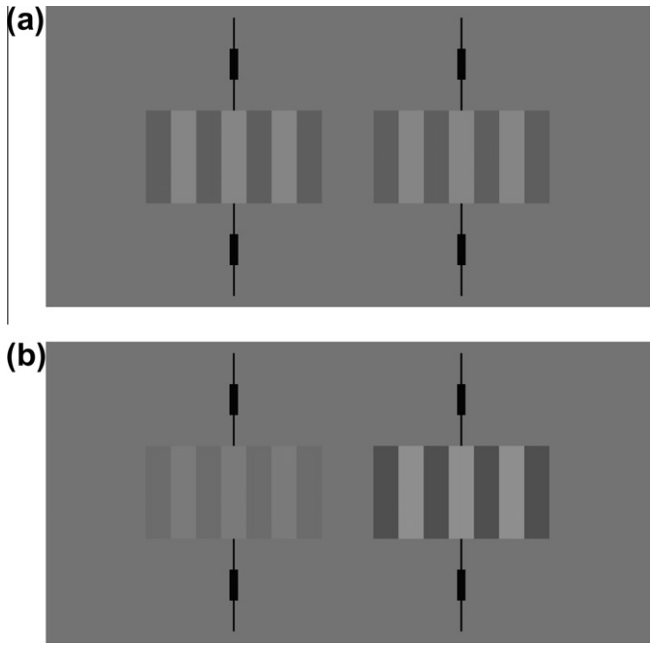

Fig. 1. (a and b) Stereograms of rectangular-wave gratings with zero geometric disparity and (a) no contrast disparity or (b) a contrast disparity corresponding to a dichoptic contrast modulation of approximately 0.6. Either crossed or uncrossed fusion is appropriate. If uncrossed fusion is used, the bars of stimulus (a) should appear to be in the fronto-parallel plane and the lighter bars of (b) will appear to rotate with their left edges closer to the viewer. If crossed fusion is used, the lighter bars of the fused image in (b) will appear to rotate with their right edges closer to the viewer.

and then an animated experimental stimulus that was also presented for 10 s. At the end of the trial, the experimental stimulus was replaced with a blank gray screen of 29 cd/m^2, the subject was prompted to make a response, a response was made, and then the next trial began.

Experimental animations in experiments one, two, and four consisted of two hundred frames with a constant average luminance with sine-wave or square-wave modulations[4] of contrast. The contrast modulation in one eye was π radians out of phase with that in the other eye. Therefore, as the stimulus contrast increased in one eye, it decreased in the other eye. The two gratings remained geometrically identical. Fig. 1b shows differences in contrast for each eye for one frame of the animation. In geometric disparity conditions used in experiment three the contrast remained constant, but the light bars of the gratings became either wider or narrower in each eye. Again, the geometric modulation in one eye was π radians out of phase with that in the other eye. The amplitude and frequency of each contrast modulation was determined for each trial by randomly choosing from a set of pre-determined values. Amplitude values represented how much of the range was covered by the modulation. Modulations with higher amplitudes had higher contrast disparity at the wave peak.

For all experiments, subjects were to respond with "1" if they saw no depth and no movement (the grating appeared to be flat), "2" if they only saw stationary depth (individual bars flipping back and forth in depth without smooth movement), and "3" if they saw the individual bars smoothly rotating back and forth (motion-in-depth).

3. Experiment one

As described above, perceived depth from a geometric retinal disparity can be seen as the frequency of depth reversals increase to slightly above 5 Hz (Beverley & Regan, 1973a, 1973b, 1974a, 1974b; Regan & Beverley, 1973a, 1973b; Richards, 1972). Experiment one measures the frequency at which a contrast disparity can be sine-wave modulated before depth from the Venetian blind effect is no longer visible. If, as suggested by irradiation, the Venetian blind effect is entirely entoptic, depth should remain visible at frequencies near 5 Hz.

3.1. Subjects

Subjects were JJD, RSH, and WWS. Subjects JJD and WWS had normal vision, while RSH had myopia, as well as a slight astigmatism in the left eye, each of which are corrected by glasses. All were experienced observers with normal stereopsis.

3.2. Apparatus

The apparatus and the stimuli consisting of stereo pairs of vertically oriented square wave gratings, as described above.

3.3. Procedure

Stimuli were constructed using modulation[4] amplitude values of 0.2, 0.4, 0.6, 0.8, and 1.0, and a range of temporal frequency values from 0.6 to 1.8 Hz in steps of 0.1 Hz (0.6, 0.7, 0.8, etc.). Contrast modulation amplitudes and frequencies were factorially combined and presented in random order during each session. Experimental animations were constructed so that contrast followed a sine wave modulation as described above. Each subject completed 65 trials in each session for two practice sessions and twelve experimental sessions.

3.4. Results

The probability of perceiving depth (one minus the probability of perceiving "no depth;" upper panels) and motion-in-depth (lower panels) is shown in Fig. 2 for each subject. Only amplitudes for which a given subject exceeded a probability of 0.75 for depth or motion-in-depth at the lowest frequency are plotted (0.6, 0.8, and 1.0 for all three subjects plus 0.4 for WWS). Standard errors are calculated using the score confidence interval (Eq. (2) from Agresti & Coull, 1998; Wilson, 1927) with $n = 12$ and $\alpha = 0.318$. The dynamic generalized-difference model, presented below, was used to generate the psychometric function curves in Fig. 2.

At lower frequencies, all subjects reported seeing individual bars of the square wave grating smoothly rotate back and forth in depth. Critical frequencies, or those frequencies that engendered a probability of 0.5, fell in a range between 1.03–1.24 Hz for the motion-in-depth response and 1.22–1.51 Hz for the depth response (Fig. 7).

3.5. Discussion

The range of frequencies for which the Venetian blind effect becomes no longer visible is less than a third that reported by previous work for oscillating geometric disparity (Beverley & Regan, 1974a, 1974b; Regan & Beverley, 1973a, 1973b; Richards, 1972). This result reinforces the view that the irradiation models proposed by Cibis and Haber (1951) and inspired by von Helmholtz (1911/1924, pp. 186–193; Filley et al., 2011) do not adequately account for perceived depth from the Venetian blind effect, as the temporal dynamics of the Venetian blind effect differ from, and are much slower than, the dynamics of geometric disparity.

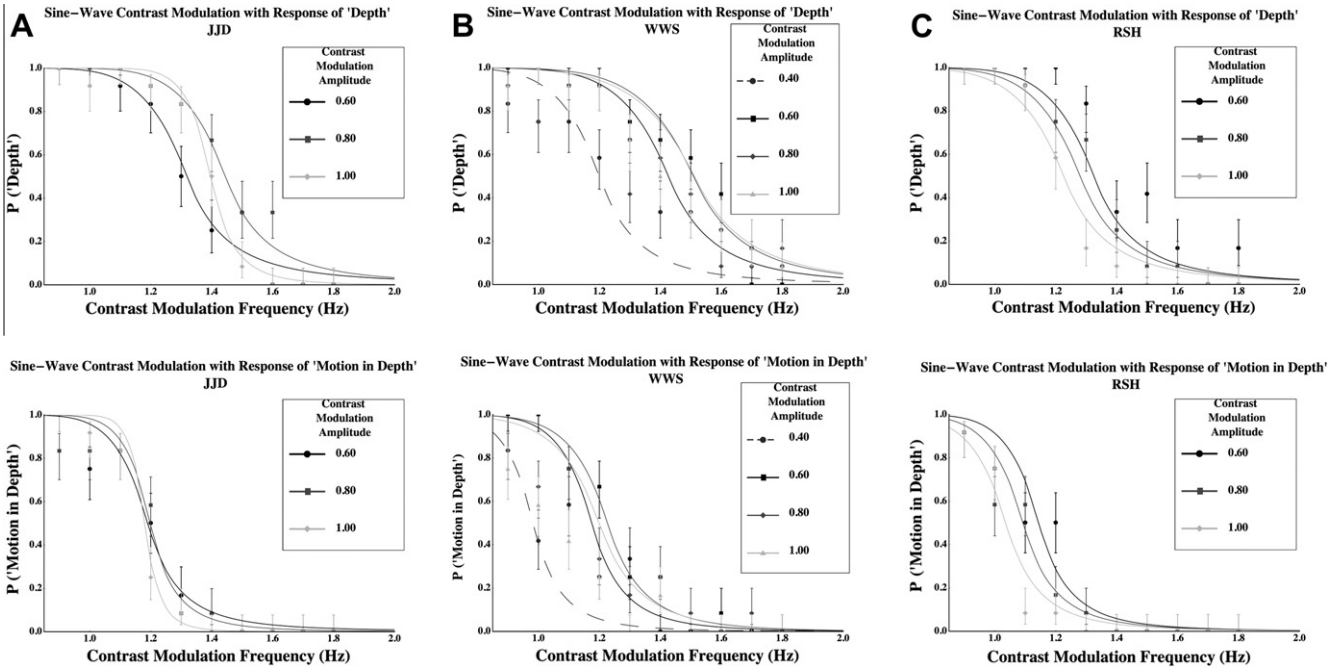

Fig. 2. (a–c) Experiment one. Probability of perceiving depth, upper panel, or motion-in-depth response, lower panel, with sine-wave contrast disparity modulations as a function of the contrast disparity modulation temporal frequency in Hertz. Plots for "depth" represent one minus the probability of perceiving "no depth." Several contrast disparity modulation amplitudes are presented. Psychometric functions are from the dynamic generalized-difference model. Standard errors are calculated using the score confidence interval (Agresti & Coull, 1998, Eq. (2); Wilson, 1927) with $n = 12$ and $\alpha = 0.318$. (a) Subject JJD. Contrast disparity amplitudes of 0.6, 0.8, and 1.0 are presented. JJD perceived depth or motion in depth with a probability below 0.75 when the contrast disparity amplitude was either 0.2 or 0.4. (b) Subject WWS. Contrast disparity amplitudes of 0.4, 0.6, 0.8, and 1.0 are presented. WWS perceived depth or motion in depth with a probability below 0.75 when the contrast disparity amplitude was either 0.2. (c) Subject RSH. Contrast disparity amplitudes of 0.6, 0.8, and 1.0 are presented. RSH perceived depth or motion in depth with a probability below 0.75 when the contrast disparity amplitude was either 0.2 or 0.4. Clearly, with two free parameters per amplitude, the model can describe the data quite well.

4. Experiment two

The results of experiment one showed that perceived depth from a contrast disparity diminished at frequencies far below 5 Hz, suggesting that the visual system processes depth from geometric and contrast disparities using different mechanisms. Experiment two replicates these findings using square wave contrast modulations. Further, since the high frequency components of the square wave contrast modulation would be above the critical frequencies found in experiment one, a low-pass linear system mapping from contrast disparity to perceived rotation would predict that the individual bars would appear to smoothly rotate back and forth (motion-in-depth) when frequencies exceed approximately 0.5 Hz.

4.1. Subjects

Subjects were JJD, RSH, WWS (described previously), and JRH. Subject JRH was not an experienced observer and was naïve with respect to the specific details and hypotheses of the experiments. JRH was myopic, which was corrected by glasses.

4.2. Apparatus

The apparatus and the stimuli, consisting of stereo pairs of vertically oriented square wave gratings, were unchanged from experiment one.

4.3. Procedure

Stimuli were constructed using amplitude values from experiment one. These were factorially combined and presented in random order during each session to JJD, RSH, WWS. JRH only viewed an amplitude of 0.6 and a frequency range with half the density of that presented to the other subjects. Square wave modulations of contrast disparity were used. Again, each subject completed 65 trials during any given session, for a total session time of approximately 35 min. Two practice sessions and 12 experimental sessions were run with JJD, RSH, and WWS.

4.4. Results

The probability of perceiving depth alone (one minus the probability of perceiving "no depth") for each subject is shown in Fig. 3. Standard errors were calculated and psychometric curves were fit in the same manner as experiment one. Critical frequencies for perceived depth for all subjects fell in a range between 1.14 and 1.46 Hz (Fig. 7), similar to those with a sine-wave contrast disparity modulation and a depth percept. No subject reported smooth motion-in-depth.

4.5. Discussion

Again, as in experiment one, the results showed that the frequency range for which the Venetian blind effect becomes no longer visible is much lower than that reported for geometric disparity (Beverley & Regan, 1974a, 1974b; Regan & Beverley, 1973a, 1973b; Richards, 1972).

That smooth motion-in-depth is visible with a sine-wave modulation and not with a square-wave modulation at, roughly, 1.1 Hz implies that our subjects would be able to discriminate the two waveforms at 1.1 Hz on the basis of perceived motion-in-depth. This result has major implications. If a low-pass linear system (e.g., Norman, 1981, Lecture 11) described perceived rotation

through the Venetian blind effect, the discrimination would have to be based on the third harmonic, at 3.0 Hz or higher, since the two waveforms have matched fundamental frequencies. But perceived motion in depth, which would be the basis of the discrimination, vanishes above about 1.1 Hz. Indeed, all perceived depth disappeared for frequencies above around 1.3 Hz. Given that monocularly-viewed temporal contrast modulations can be perceived at frequencies greater than 10 Hz (Kelly, 1979), it seems likely that such a discrimination is based on monocularly available contrast changes that feed into the binocular locus responsible for perceived rotation but that this input is gated by a process with a critical frequency of about 1.3 Hz. We explore these ideas more fully using the gated generalized difference model below.

5. Experiment three

Experiments one and two both showed that perceived depth from a contrast disparity diminishes before the depth reversals reach 1.5 Hz, which is one third the frequency at which depth remains visible when viewing geometric disparity modulations (Beverley & Regan, 1973a, 1973b, 1974a, 1974b; Regan & Beverley, 1973a, 1973b; Richards, 1972). However, the stimuli used in experiments one and two are very different from those used previously by others. Therefore, experiment three uses square wave gratings manipulated to increase the width of the light bars in one eye while all bars remain equal width in the other eye. Depth should remain visible as the frequency of depth reversals approach 5 Hz.

5.1. Subjects

Subjects were RSH, JJD, WWS, and JRH, who were described previously.

5.2. Apparatus

The computer, display monitor, and software were the same as was described previously. Stimuli were stereo pairs of vertically oriented square wave gratings. The width of the three lighter bars were dynamically altered in a square wave manner to be wider in one eye than in the other, creating geometric disparities. Each pixel of a dark bar that was adjacent to a light bar edge in experiment one was varied to be either lighter or darker. Each of the pixels that could vary began a trial at the average luminance in both monocular images. The luminance of each pixel was increased to the luminance of the lighter bars in one monocular

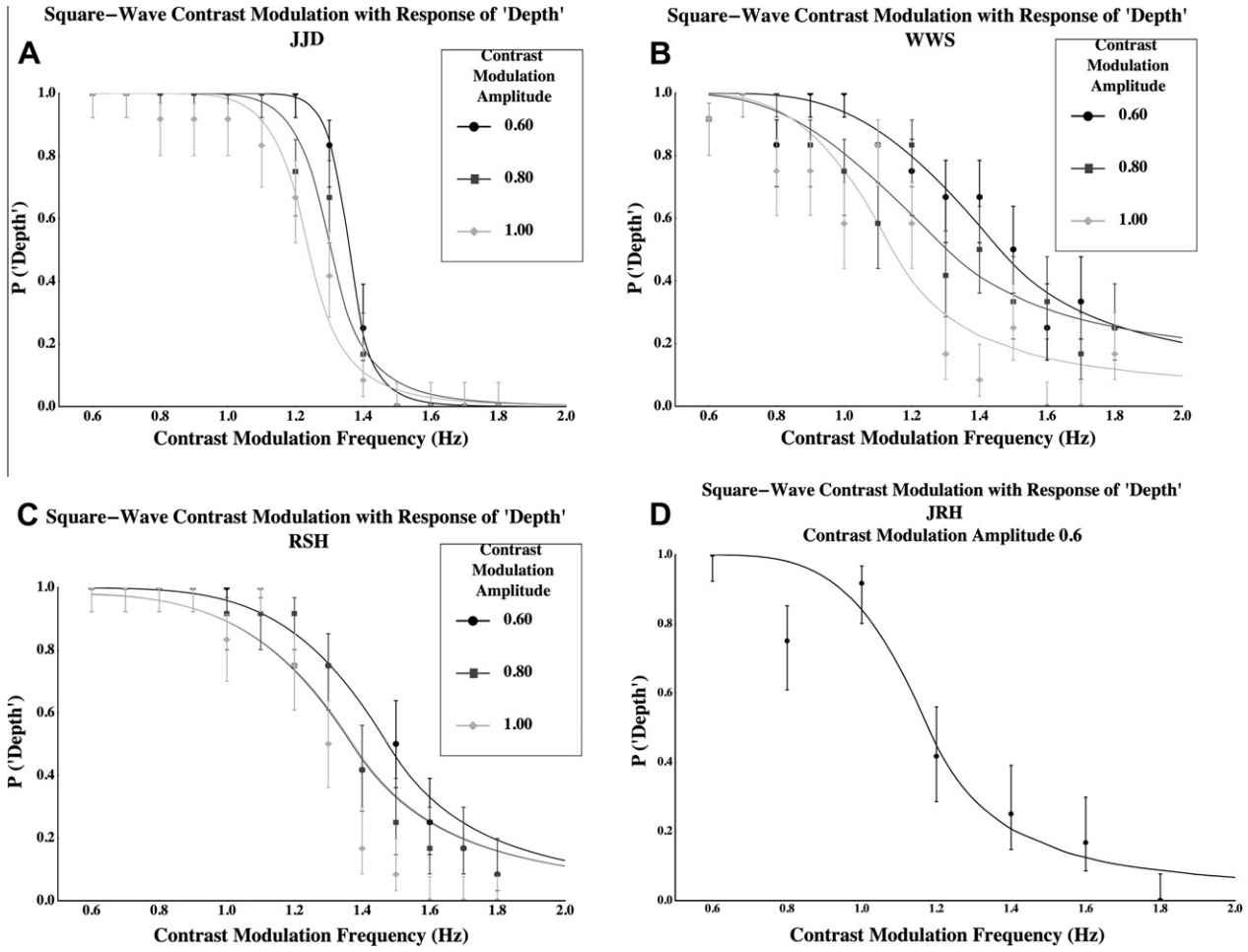

Fig. 3. (a–d) Experiment two. Probability of perceiving depth (one minus the probability of perceiving "no depth") with square-wave contrast disparity modulations as a function of the contrast disparity modulation temporal frequency in Hertz. Contrast disparity amplitudes of 0.6, 0.8, and 1.0 are presented. Depth was perceived with a probability below 0.75 when the contrast disparity amplitude was either 0.2 or 0.4 by all three subjects. Psychometric functions are from the dynamic generalized-difference model. Standard errors are calculated using the score confidence interval (Agresti & Coull, 1998, Eq. (2); Wilson, 1927) with $n = 12$ and $\alpha = 0.318$. (a) Subject JJD. (b) Subject WWS. (c) Subject RSH. (d) Subject JRH. Again, with two free parameters per amplitude, the model can describe the data quite well.

image, while being decreased to the luminance of the darker bars in the other monocular image, creating the appearance of individual bars increasing and decreasing in size in a square wave motion. Upon fusion, the stereo pair appeared to rotate from the plane in a square-wave motion. The angular disparity of each edge of the lighter bars was about 37.8 s of arc (giving a horizontal size ratio of the lighter bars was approximately 1.05), which is that needed to cancel the rotation perceived when viewing a contrast modulation of approximately 0.92 (Hetley & Stine, 2011).[4] The amount of perceived rotation caused by increasing the size of the lighter bars by two pixels in one eye corresponded to that seen in the Venetian blind effect with the contrast modulations that were used. When the lighter bars were altered to be wider in one eye, each individual light bar was 1.6° in height and 0.431° in width. The overall monocular image remained 1.6° in height and 2.8° in width.

5.3. Procedure

The frequency of width change ranged from 0.2 to 5.0 Hz in steps of 0.2 Hz (0.2, 0.4, 0.6, 0.8, etc.), in random order. Again, JRH only viewed a frequency range with half the density of that presented to the other subjects. Each experimental session consisted of four choices at each frequency value. Subjects RSH, JJD, WWS completed two sessions for a total of eight choices at each frequency. Each session was one hundred trials, for a session time of approximately 45 min.

5.4. Results

The probability of perceiving depth is shown in Fig. 4 for all subjects. Standard errors were calculated and psychometric curves were fit in the same manner as experiments one and two. The data from Fig. 3, experiment two, are plotted in gray for comparison.

The range of critical frequencies for perceived depth for all subjects was much higher than in conditions of contrast disparity (3.61–5.50 Hz; Fig. 7).

5.5. Discussion

Our results replicate those of previous research with geometric disparities (Richards, 1951, 1972; Beverley & Regan, 1974a, 1974b; Regan & Beverley, 1973a, 1973b). The probability of perceiving depth decreased as the frequency increased, but was still reported frequently at 4.8 Hz. This result suggests that perceived depth from the Venetian blind effect, which diminishes at frequencies above 1.3 Hz (experiments one and two), is processed by mechanisms that differ from those processing geometric disparities.

One might argue that the large difference in processing speed between contrast and geometric disparities was due to eye movements induced by contrast disparity changes. If a contrast disparity change causes a saccade, any depth or motion-in-depth occurring during the saccade may not be perceived due to saccadic suppression (e.g. Bridgeman, Hendry, & Stark, 1975).

As contrast disparity increases, perceived binocular visual direction perceptually shifts towards the higher contrast monocular image (Mansfield & Legge, 1996; Weiler, Maxwell, & Schor, 2007), and the oculomotor system uses contrast disparity to guide binocular saccades towards the perceived binocular visual direction (Weiler, Maxwell, & Schor, 2007). However, in the absence of geometric disparities, binocular saccade amplitude is independent of contrast disparity (Weiler, Maxwell, & Schor, 2007). Further, the frequency at which depth was no longer visible in all contrast disparity conditions was approximately 1.0 to 1.5 Hz, or 667–1000 ms per cycle. These durations are well below the roughly 100 ms expected through saccadic suppression (e.g. Bridgeman, Hendry, & Stark, 1975).

6. Experiment four

Results from experiments one and two and subjects' reports suggested that subjects were able to discriminate sine and square wave depth modulations at 1 Hz on the basis of perceived motion in depth. As mentioned previously, if a linear system described perceived rotation through the Venetian blind effect, the discrimination would have to be based on the third harmonic. But perceived motion in depth vanishes above about 1.1 Hz. We directly measured the ability of subjects to discriminate a sine-wave depth modulation from a square-wave depth modulation by asking subjects to identify whether or not they perceived motion in depth, depth with no motion, or no depth in order to validate our inference that such discriminations are possible at 1 Hz.

6.1. Subjects

Subjects were JJD and JRH (described above). Again, JRH was naïve with respect to the hypotheses that we tested.

6.2. Apparatus

The apparatus and the stimuli, consisting of stereo pairs of vertically oriented square wave gratings, were unchanged from experiments one through three.

6.3. Procedure

Procedures for experimental setup and individual experimental sessions were the same as in experiments above. Each experimental session tested sine and square wave contrast modulations at six different frequencies and one amplitude value of 0.68. Frequencies were 0.6, 0.8, 1.0, 1.2, 1.4, and 1.6 Hz. As before, subjects were asked to make one of three possible choices "motion in depth," "depth with no motion," or "no depth." A choice of motion in depth indicated that subjects perceived smooth sine wave depth modulations. However, a response of depth with no motion indicated the perception of square wave depth modulations. Experimental sessions consisted of 60 total trials. Each subject completed four sessions for a total of 20 choices at each frequency/type of modulation combination.

6.4. Results

Fig. 5 shows the probability of perceiving motion in depth with a sine wave (black, solid), motion in depth with a square wave (black, dashed), depth with a sine wave (gray, solid), and depth with a square wave (gray, dashed) for JRH (top) and JJD (bottom). For both subjects, motion in depth was reported for sine wave modulations but not for square wave modulations and the probability of perceiving depth fell below threshold at frequencies below 1.4 Hz.

6.5. Discussion

Results showed that subjects perceived smooth motion in depth with a sine wave modulation and sharp depth changes with square wave modulations. Further, results replicated experiments one and two, where the probability of perceiving depth diminished for both sine and square wave modulations at frequencies below 1.4 Hz. It is clear that subjects are able to discriminate the pattern of

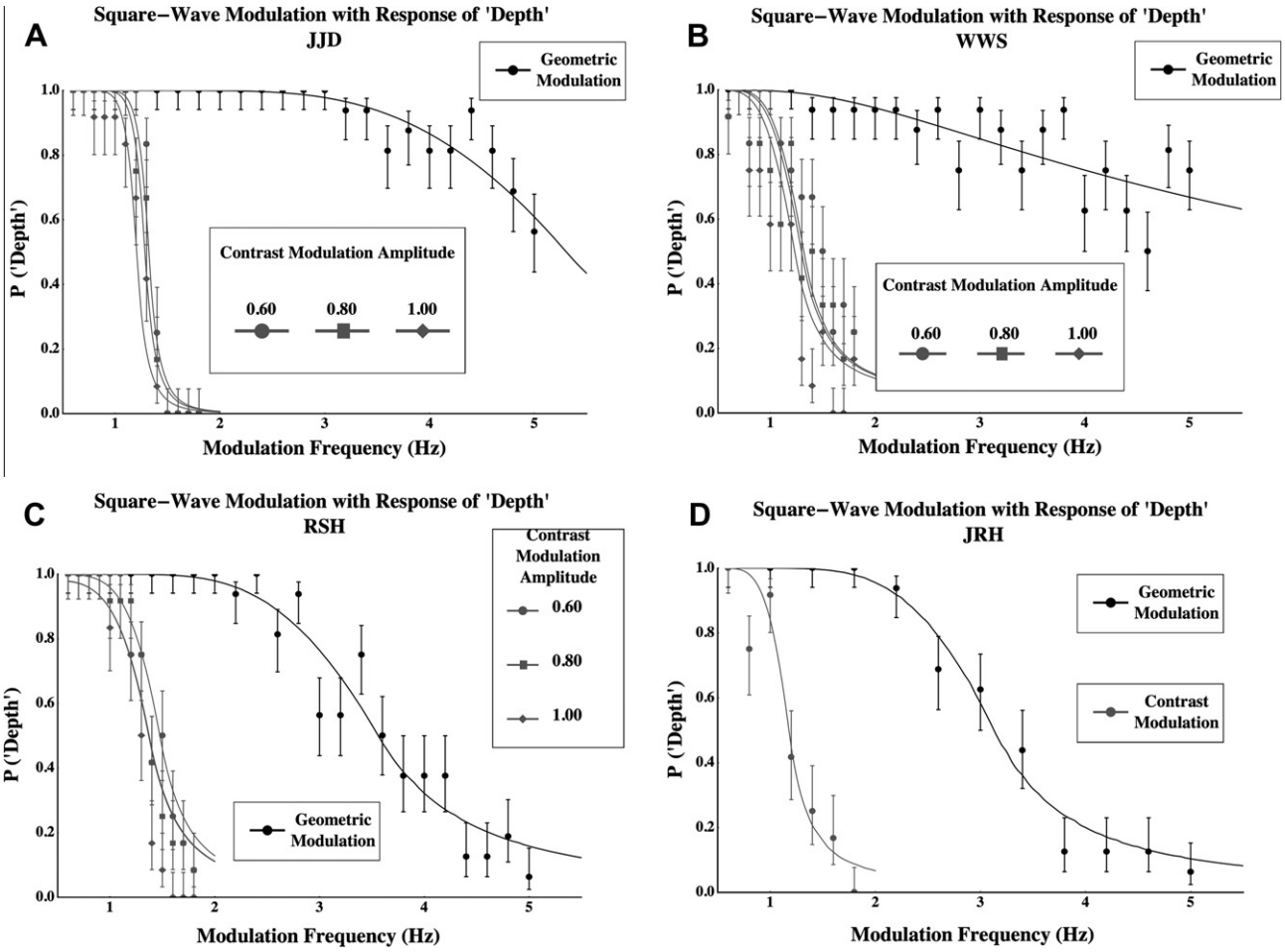

Fig. 4. (a–d) Experiment three. Probability of perceiving depth (one minus the probability of perceiving "no depth") with square-wave geometric disparity modulations as a function of the geometric disparity modulation temporal frequency in Hertz. Psychometric functions are from the dynamic generalized-difference model. Standard errors are calculated using the score confidence interval (Agresti & Coull, 1998, Eq. (2); Wilson, 1927) with $n = 12$ and $\alpha = 0.318$. For comparison, data from experiment two, Fig. 3, are presented in gray (a) Subject JJD. (b) Subject WWS. (c) Subject RSH. (d) Subject JRH. Yet again, with two free parameters for the geometric disparity data, the model can describe the data quite well.

perceived rotation engendered by sine- and square-wave contrast disparity modulations close to the critical frequency.[5]

7. Modeling the temporal dynamics of the Venetian blind effect

7.1. Introduction

A model of the dynamic aspects of the Venetian blind effect was developed. Our goal was to capture (i) the critical frequencies measured for the contrast and geometric disparity modulations, with the extremely sharp drop in the probability for perceiving rotation at the critical frequency with a contrast modulation, and (ii) the proximity of the critical frequency to detect depth with contrast disparity modulations to the critical frequency to discriminate between perceived rotation engendered by a sine-wave from a square-wave modulation. We wished to capture these results with a model that was a straight-forward generalization of the difference models explored by Filley et al. (2011) and Hetley and Stine (2011) while using as few free parameters as possible. Successfully capturing these results would suggest that they can be described relatively simply. A failure would call into question the difference models. A few alternative models are discussed in Section 7.6.

Consistent with the models presented in Filley et al. (2011) and Hetley and Stine (2011), the existence of a single locus (Teller, 1984) was assumed (the cyclopean locus) for the perception of rotation into which both geometric and contrast disparities feed. Results showing that both average luminance disparities (Cibis & Haber, 1951; Hetley & Stine, 2011) and contrast disparities (Hetley & Stine, 2011) can cancel perceived rotations created using a geometric disparity are consistent with the single-locus assumption. Further, we assumed that input channels supporting contrast disparities differ from those supporting geometric disparities.

Given that we have two monocular channels carrying contrast information from each eye into the cyclopean locus, we assume that these monocular contrast channels register the contrast across vertically oriented edges in the image on corresponding locations of each retina (we have not explored the case where edges are

[5] As a check, we presented either sine-wave or square-wave contrast disparity modulations at 1.0 Hz to four subjects who were to report "motion-in-depth" or "no motion-in-depth." Each subject (JJD, WWS, ALC, and PCN), two of which were naive (ALC and PCN), ran one session making 30 judgments about sine-wave modulations and 30 judgments about square-wave modulations that were randomly interleaved. Probability for "motion-in-depth" with the sine-wave modulation were JJD: 1.0, WWS: 1.0, ALC: 0.967, and PCN: 0.933. Probability for "motion-in-depth" with a square-wave modulation was 0.0 for all four subjects. Clearly subjects can discriminate a sine-wave contrast disparity modulation from a square-wave based on perceived rotation with little difficulty. We did not ask subjects to only discriminate the contrast disparity modulations, rather than perceived rotations. However, when viewing the stimulus, it seems very clear that one can discriminate a sine-wave contrast disparity modulation from a square-wave contrast disparity modulation with ease at frequencies well above 1.2 Hz (i.e., when no rotation is perceived).

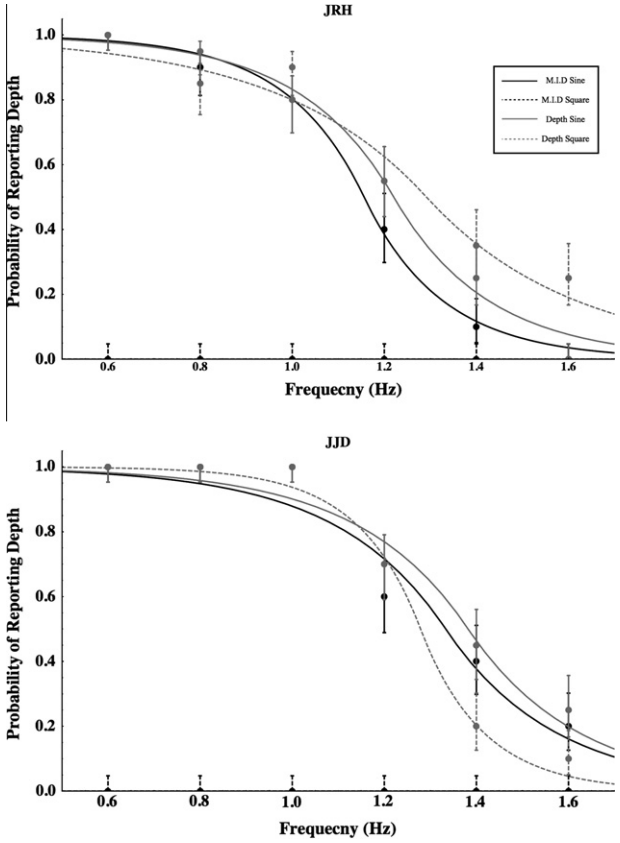

Fig. 5. Experiment four. Probability of perceiving motion-in-depth with a sine wave depth modulation (black, solid), motion-in-depth with a square wave depth modulation (black, dashed), depth with a sine wave depth modulation (gray, solid), and depth with a square wave depth modulation (gray, dashed) for JRH (top) and JJD (bottom). Plots for "depth" represent one minus the probability of perceiving "no depth." Probabilities of perceiving "depth but no motion" are not plotted.

not essentially vertical, except to note that horizontal edges are unnecessary; Filley et al., 2011). They have time constants that are small relative to stereopsis, leading to high critical frequencies (e.g., Ikeda, 1986; Kelly, 1979), and they are distinct from channels that carry monocular information used for local stereopsis through geometric disparities (e.g., Chen & Qian, 2004), which we call monocular local edge channels. The cyclopean locus has time constants engendering critical frequencies in the range of 4.8 Hz and, we assume, receives inputs from both the monocular contrast channels and the monocular local edge channels. The nature of the inputs from the monocular local edge channels will not be considered in detail since an enormous amount of theoretical work has already gone into understanding these inputs (e.g., Chen & Qian, 2004; cf., Filley et al., 2011). The monocular contrast channels are presumed to feed into the cyclopean locus with opposing polarities. So, when viewing the image in Fig. 1b, the two contrast channels, one from each eye, would generate differing outputs due to the contrast disparity in the dichoptic stimulus (Filley et al., 2011; Hetley & Stine, 2011). A geometric disparity could be introduced in order to cancel perceived rotation due to the contrast disparity (Hetley & Stine, 2011). Note that the contrast edges are defined monocularly. Hence, the Venetian blind effect fails with random-dot stereograms (Filley et al., 2011). Further, the contrast at each edge is assumed to be roughly in the linear range of the compressive nonlinearity (Filley et al., 2011). A similar model, we presume, accounts for the effects of an average luminance disparity (Cibis & Haber, 1951; Filley et al., 2011; Hetley & Stine, 2011).

Experiments one, two, and four show that a linear dynamical system cannot account for our results. At 1 Hz, for example, a subject can discriminate a square-wave temporal modulation from a sine-wave modulation by responding to perceived depth or motion in depth. Such a discrimination must be based on information carried at a frequency of about 3 Hz or greater. Both the monocular contrast channels and the cyclopean locus can carry information at that frequency. However, perceived depth engendered by a contrast disparity modulation evaporates at around 1.3 Hz. Some sort of gating mechanism, we presume, shuts down the transmission of perceived rotation as a function of contrast disparities when the frequency of the modulation exceeds 1.3 Hz.

We begin by fitting the dynamic generalized difference model to the psychometric functions for the depth response from experiments one through three. Then we model perceived rotation with the addition of a gating mechanism in order to address the motion-in-depth results from experiments one, two, and four. The dynamic model consists of a system of three differential equations. Two equations describe the input to the cyclopean locus from the two eyes in response to the contrasts of the stimuli presented dichoptically, the monocular contrast channels. The third describes the response at the cyclopean locus, effectively, to the difference in the response from the first two equations. Given the first assumption, that a single locus controls the perception of rotation, data from experiment three are used to define the parameters for the third member of the system, which describes the temporal characteristics of the cyclopean locus. Conditional upon that result, parameters are defined describing the input from the first two members of the system to the third using data from experiments one and two.

The system is a straightforward generalization of the model developed by Hetley and Stine (2011). The generalization follows three paths. The first generalizes the notion of a difference between the response to contrast across corresponding vertical edges from the two eyes in order to account for the greater range of contrasts used in the present experiments. The second is intended to capture the temporal, or dynamic, aspects of the Venetian blind effect. The third concerns the gating mechanism in order to account for the observation that a sine-wave temporal contrast modulation can be discriminated from a square-wave contrast modulation at a frequency only slightly below the critical frequency for detecting depth through the Venetian blind effect. The development of the generalized difference is described in Appendix A.

7.2. The dynamic generalized-difference model

The perceived edge shift in response to a contrast disparity is modeled using a system of three differential equations,

$$\begin{cases} \frac{df_l(t)}{dt} = \frac{1}{\tau}(-f_l(t) + R(C_l(t))) \\ \frac{df_r(t)}{dt} = \frac{1}{\tau}(-f_r(t) + R(C_r(t))) \\ \frac{dg(t)}{dt} = \frac{1}{\tau_{cyc}}(-g(t) + gain(f_l(t) - f_r(t))(f_l(t) - M)(f_r(t) - M)) \end{cases}, \quad (1)$$

where the contrast of the grating presented to a particular eye, $C_{eye}(t)$, changes as a function of time, $R(C_{eye}(t))$ is the Naka-Rushton equation (Naka & Rushton, 1966; see Eq. (A1)) and describes the steady-state response of a cell to contrast, $f_{eye}(t)$ describes the dynamic neural response to the contrast presented to a given eye, incorporating $R(C_{eye}(t))$, τ is the time constant for the neural response to contrast for either eye, $g(t)$ is the cyclopean perceived disparity of the particular edges of the bars composing the rectangular-wave grating, M is defined with respect to Eq. (A1), *gain* is the parameter controlling the strength of the input from the generalized difference in neural response to the grating pairs, and, finally, τ_{cyc} is the time constant for the cyclopean response.

System of Eq. (1) can be solved using standard techniques with boundary conditions $f_{eye}(0) = 0$ impulses/s (imp/s) and $g(1) = 0^\circ$ of

visual angle (deg). The result is one equation describing the neural response to the contrast of a rectangular-wave grating presented to a given eye, $f_{eye}(t)$, and a second equation, $g(t)$, describing the perceived disparity at the edge of each bar in response to the generalized difference between $f_l(t)$ and $f_r(t)$. The neural response to the contrast of a rectangular-wave grating presented to one eye is

$$f_{eye}(t) = Me^{-\frac{t}{\tau}} + \frac{1}{\tau}\int_0^t e^{\frac{t'-t}{\tau}} R(C_{eye}(t'))dt' \tag{2}$$

where $R(C_{eye}(t))$ is again defined by Eq. (A1) and τ is the time constant for the neural response to contrast for either eye. The perceived disparity at the edge of each bar in response to the generalized difference between $f_l(t)$ and $f_r(t)$, is

$$\begin{aligned} g(t) = -gain\frac{e^{-\frac{t}{\tau_{cyc}}}}{\tau_{cyc}}\int_1^t e^{t_3\left(\frac{1}{\tau_{cyc}}-\frac{2}{\tau}\right)}\left(\frac{1}{\tau}\int_0^{t_3} e^{\frac{t_1}{\tau}}R(C_l(t_1))\mathrm{d}t_1\right. \\ \left.+\frac{1}{\tau}\int_0^{t_3} e^{\frac{t_2}{\tau}}R(C_r(t_2))\mathrm{d}t_2\right)((e^{\frac{t_3}{\tau}}-1)M+\frac{1}{\tau}\int_0^{t_3} e^{\frac{t_1}{\tau}}R(C_l(t_1))\mathrm{d}t_1) \\ \times\left(\left(e^{\frac{t_3}{\tau}}-1\right)M+\frac{1}{\tau}\int_0^{t_3} e^{\frac{t_2}{\tau}}R(C_r(t_2))\mathrm{d}t_2\right)\mathrm{d}t_3 \end{aligned} \tag{3}$$

where *gain* is the parameter controlling the strength of the input from the generalized difference in neural response to the grating pairs, τ_{cyc} is the time constant for the cyclopean response, and the other symbols are as defined for Eq. (2). Finally, perceived horizontal size ratio can now be defined as

$$PercHSR(C_l(t), C_r(t)) = \frac{width + 2g(t)}{width - 2g(t)}, \tag{4}$$

where *width* is the width of each bar of the rectangular wave grating, and $g(t)$ is defined by Eq. (3). Note that, in our implementation, if the lighter bars are perceived as figure, then *width* corresponds to the width of the lighter bars. Similarly, if the darker bars are perceived as figure, then *width* corresponds to the width of the darker bars. Filley et al. (2011) remark that the Venetian blind effect may be viewed with either the lighter bars or the darker bars perceived as figures.

Eq. (4) is used to describe the perceived rotation of the individual bars of the rectangular-wave grating in response to a contrast disparity. A Laplace distribution, which is a consequence of the intensity difference model (Filley et al., 2011), is used to calculate response probabilities from Eq. (4).

Due to the use of a generalized difference in the system of Eq. (1), as the contrast of a grating presented to one eye approaches zero, only the higher contrast grating remains visible, bringing perceived rotation to zero given that our stimuli appear to lie in a fronto-parallel plane when viewed monocularly or binocularly with no contrast disparity. The shift in the perceived location of each edge in a rectangular-wave grating as a function of contrast disparity, Eq. (3), is used to calculate a perceived horizontal size ratio (Eq. (4)), thereby generating an asymmetry in perceived horizontal size ratio as a function of contrast disparity.

7.3. The gated dynamic generalized-difference model

Again, the results from experiments one, two, and four imply that our subjects can discriminate a square-wave contrast disparity modulation from a sine-wave contrast disparity modulation on the basis of perceived motion-in-depth when the frequency of the modulation is below about 1.1 Hz and all perceived depth disappears at frequencies exceeding approximately 1.3 Hz. Hence, information concerning the change in monocular contrast, and presumably luminance, must be used to determine the perceived change in rotation.

This conclusion leads to the gated dynamic generalized difference model. Conceptually, the perceived edge shift magnitude is driven by the generalized inter-ocular difference in contrast gated by the temporal properties implied by Eq. (3). There are a number of ways to mathematically realize such a model. Eq. (5) presents one possibility. Perceived edge shift, $p(t)$, is modeled as the product of the inter-ocular generalized difference in contrast and the magnitude of the generalized difference model integrated over a single period of the stimulus at the critical frequency.

$$p(t) = gain(f_l(t) - f_r(t))(f_l(t) - M)(f_r(t) - M)\int_{t-\frac{1000}{\omega}}^{t} |g(t')|dt', \tag{5}$$

Hence, the generalized difference model describes perceived edge shift from Eq. (3) and the resulting perceived horizontal size ratio change from Eq. (4) while the gated generalized difference model describes perceived edge shift from Eq. (5) and the resulting perceived horizontal size ratio change from Eq. (4) with, of course, $p(t)$ substituted for $g(t)$.

7.4. Fitting the models

We fit the generalized difference model to the data from experiments one through three, and then fit the gated generalized difference model using the parameters from the generalized difference model to account for the motion-in-depth results. Following Hetley and Stine (2011), the parameters for the Naka-Rushton equation (Eq. (A1)) were set to the values used by Sclar, Maunsell, and Lennie (1990) to describe V1 cells in *Macaca fascicularis*. Hence, all of these parameter values were defined independently of our data.

The remaining three parameters, τ_{cyc}, τ, and σ_ε, were fit sequentially to data from each subject, where σ_ε is the standard deviation for the Laplace distribution. First, for a given subject, the least-squares values for τ_{cyc} and σ_ε were found to predict that subject's probability of seeing depth from geometric modulations as measured in experiment three. During this step $\tau = \tau_{cyc}/100$, thereby effectively giving a value for τ_{cyc} that reflects the time limits imposed at the cyclopean locus. The psychometric functions plotted in Fig. 4 for the geometric disparities are the result of these fits. Next, the least-squares fits of psychometric functions was calculated for the three largest amplitudes from the sine-wave and square-wave contrast disparity modulation experiments using τ and σ_ε while using τ_{cyc} from that subject's geometric fit. Recall that at least one subject failed to perceive depth for each of the two smaller amplitudes. Hence, two parameters, τ_{cyc} and σ_ε, were used to fit the geometric data from each subject and then two more parameters, τ and σ_ε, were used to fit each of the three largest amplitudes for the sine-wave and square-wave contrast modulation psychometric functions. For each subject, 14 parameters were used to fit the seven psychometric functions plotted in Figs. 2–4.

The psychometric functions for the motion-in-depth response to the sine-wave contrast modulations of experiment one were then fit using the parameters from the depth response while allowing the threshold perceived horizontal size ratio to deviate from 1.05. Hence, conditional upon the fit of the three psychometric functions to the depth response data from experiment one, three perceived horizontal size ratio parameters were used to fit the three psychometric functions to the motion-in-depth response data across the three largest contrast modulation amplitudes for each subject. Details of the procedure used to fit the model are presented in the Appendix B.

Conceptually, the model stipulates that just three parameters, the geometric disparity time constant τ_{cyc}, the contrast disparity

time constant, τ, and the perceived horizontal size ratio standard deviation, σ_ε, should suffice in order to describe the three psychometric functions defined by the depth response to contrast disparity modulations for each of the three subjects. In addition, a threshold shift should be sufficient to encompass the psychometric functions defined by the motion-in-depth response for each subject. To test these hypotheses, analyses of variances (ANOVAs) were conducted on the parameter estimates.

Finally, a randomized-block factorial ANOVA was conducted on the logarithm of the critical frequencies (that modulation frequency that engenders a probability of seeing depth equal to 0.50). As stated previously, the critical frequency for a geometric modulation was clearly higher than that for a contrast modulation. Further, the variability among the geometric disparity modulations across subjects was greater than for the contrast disparity modulations (see Fig. 7). Hence, only the contrast modulation critical frequencies were used for this analysis. Whether or not critical frequencies would vary across either the type of contrast modulation or the modulation's amplitude was open. It was expected that the critical frequencies for motion-in-depth with the sine-wave contrast disparity modulation to be less than that for the depth response.

Details, assumption checks, and quantitative results for the ANOVAs are presented in the Appendix C.

7.5. Results

The time constants τ and the standard deviations σ_ε differed across subjects but not across modulation type, amplitude, or their combinations. Perceived horizontal size ratio threshold parameters did not differ across subjects or contrast modulation amplitudes.

The averages across subjects of the time constants τ, standard deviations σ_ε, and perceived horizontal size ratio threshold parameters with 95% confidence intervals (defined as $\hat{\mu} \pm t_{\alpha_{familywise}/2;\nu_{residual}} \sqrt{\frac{MSRES}{3}}$; Loftus & Masson, 1994) are plotted in Fig. 6a–c, respectively. Mean critical frequencies with 95% confidence intervals (Loftus & Masson, 1994) are plotted in logarithmic coordinates in Fig. 7.

Motion-in-depth. In order to demonstrate the conundrum raised by the motion-in-depth critical frequencies, we generated predicted perceived rotations for a single stimulus presentation using the dynamic generalized difference model and the gated generalized difference model. The former model shows perceived rotations that are essentially indiscriminable for square-wave and sine-wave modulations while the later shows perceived rotations with infinite slope in response to the square-wave and finite slope in response to the sine-wave modulations.

Fig. 8 plots the perceived rotation as a function of both a square-wave contrast disparity modulation and a sine-wave contrast disparity modulation with an amplitude of 0.6 and a frequency of 1.0 Hz. The upper panel shows the prediction of the generalized difference model (where perceived edge shift is from Eq. (3), the resulting perceived horizontal size ratio change is from Eq. (4), and perceived rotation is from Eq. (B1)) and the lower panel that of the gated generalized difference model (where perceived edge shift is from Eq. (5), the resulting perceived horizontal size ratio change is from Eq. (4), and perceived rotation is from Eq. (B1)). Again, the detailed description of fitting the model is presented in Appendix B.

As expected, the generalized difference model predicts that the perceived motion-in-depth of the bars with a square-wave contrast disparity modulation should be not be distinguishable from that with a sine-wave contrast disparity modulation. However, the gated model predicts no perceived motion-in-depth with a square-wave modulation (the slope of the perceived rotation curve is essentially infinite) and perceived motion-in-depth with a sine-wave modulation.

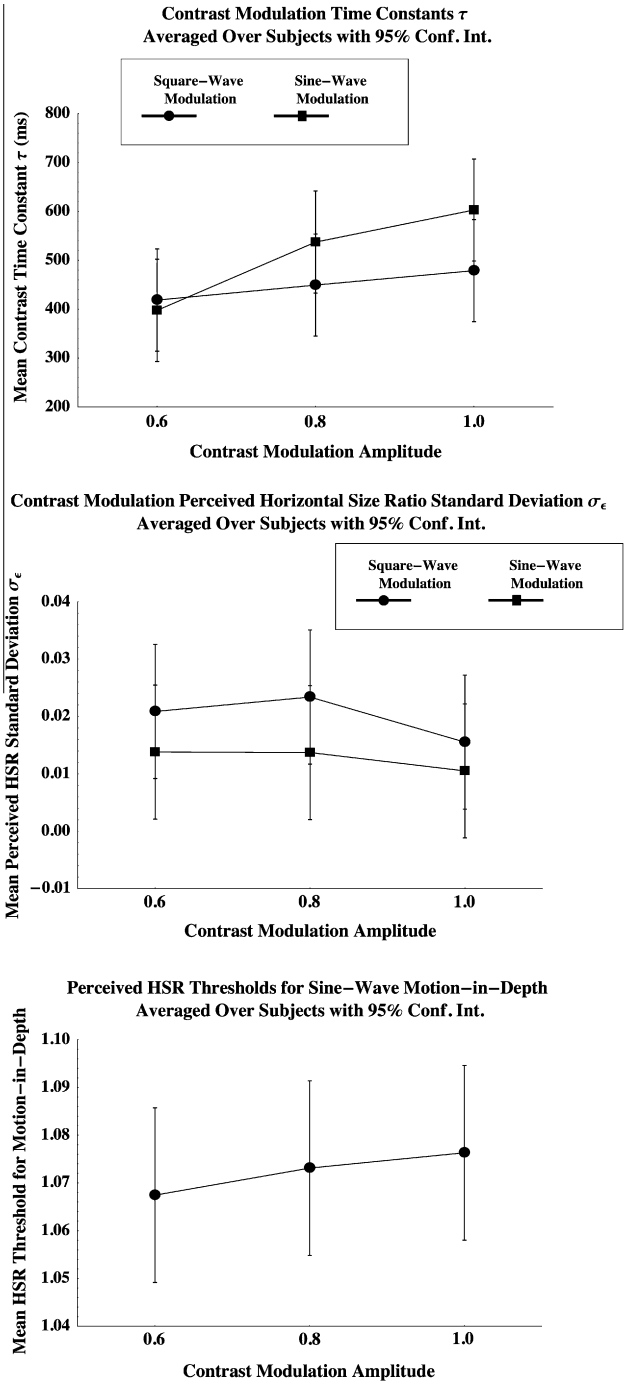

Fig. 6. Dynamic generalized-difference model parameters. The model was fit to the depth, for (a) and (b), and motion-in-depth, for (c), probabilities of perception individually for each subject (JJD, WWS, and RSH) and for contrast disparity modulation amplitudes 0.6, 0.8, and 1.0, as a function of contrast disparity modulation temporal frequency. All plots show parameter values averaged across three subjects for particular contrast disparity modulation amplitudes, waveforms, and response types. Error bars are calculated using ANOVA-based confidence intervals (Loftus & Masson, 1994) with $n = 3$ and $\alpha = 0.05$. None of the effects plotted are significant. (a) Contrast disparity modulation time constants τ (see Eq. (5)). (b) Perceived horizontal size ratio standard deviation σ_ε. (c) Perceived horizontal size ratio threshold for a motion-in-depth response. That no differences were found among these three sets of parameters together with the quality of the psychometric function fits in Figs. 2–4 suggests that the dynamic generalized-difference model captures the systematic variation in our data parsimoniously.

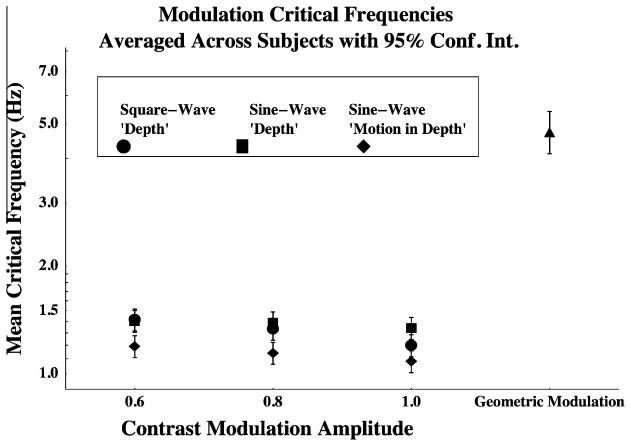

Fig. 7. Critical frequencies as a function of disparity type and contrast disparity modulation amplitude with dynamic generalized-difference model predicted critical frequencies. Data points are critical frequencies averaged across JJD, WWS, and RSH for a geometric disparity modulation and contrast disparity modulations of amplitude 0.6, 0.8, and 1.0 with 95% ANOVA-based confidence intervals (Loftus & Masson, 1994). Lines represent predicted critical frequencies from the dynamic generalized-difference model using the average cyclopean time constant τ_{cyc}, the average contrast disparity modulation time constant τ, and the average perceived horizontal size ratio standard deviation σ_ε for the depth response with both a square-wave or sine-wave contrast disparity modulation, and the average perceived horizontal size ratio threshold for the motion-in-depth response with a sine-wave contrast disparity modulation. Note that the model fits the critical frequencies reasonably well given that, (i) τ_{cyc} was fit to the geometric disparity critical frequency, (ii) six points depth response critical frequencies are approximated by the model with two free parameters, τ and σ_ε, and (iii) the three motion-in-depth response critical frequencies are fit with one additional parameter, the average perceived horizontal size ratio threshold for the motion-in-depth response. Obviously, allowing, say, the semi-saturation constant from Eq. (A1) to vary greatly enhances the fit.

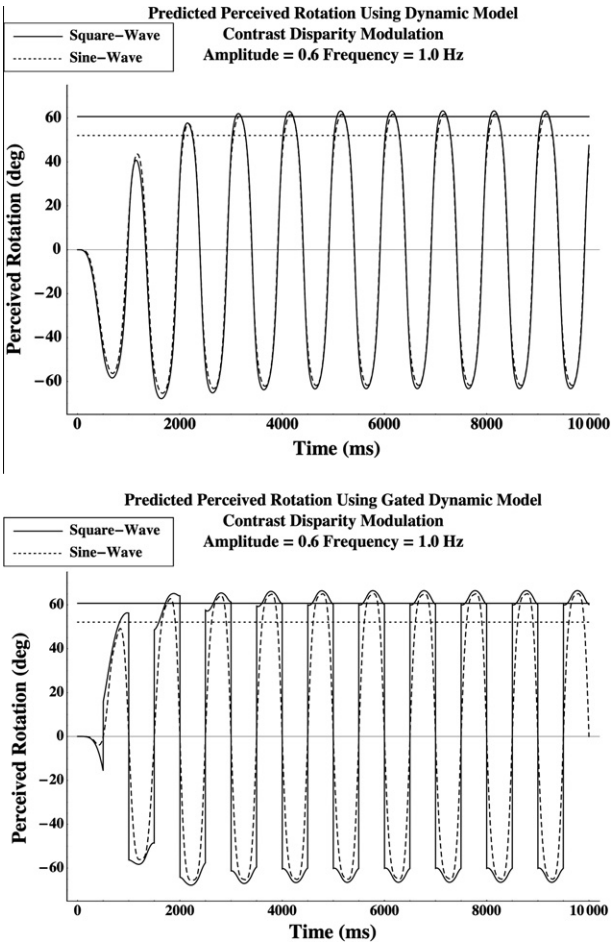

Fig. 8. Perceived rotation as a function of both a square-wave contrast disparity modulation and a sine-wave contrast disparity modulation with an amplitude of 0.6 and a frequency of 1.0 Hz. The upper panel shows the prediction of the generalized difference model (where perceived edge shift is from Eq. (3), the resulting perceived horizontal size ratio change is from Eq. (4), and perceived rotation is from Eq. (B1)) and the lower panel that of the gated generalized difference model (where perceived edge shift is from Eq. (5), the resulting perceived horizontal size ratio change is from Eq. (4), and perceived rotation is from Eq. (B1)). The generalized difference model predicts that the perceived motion-in-depth of the bars with a square-wave contrast disparity modulation are similar to that with a sine-wave contrast disparity modulation, but the gated model predicts no perceived motion-in-depth with a square-wave modulation (the slope of the perceived rotation curve is essentially infinite) and perceived motion-in-depth with a sine-wave modulation.

7.6. Discussion

We have presented two models, the generalized difference model and the gated generalized difference model. Both models posit that the generalized inter-ocular difference in contrast across vertically-oriented, corresponding edges controls perceived rotation. This difference is generalized in the sense that it approaches zero when the interocular difference in contrast approaches zero or when the contrast presented to either eye becomes small relative to that presented to the other eye, accounting for interocular suppression with large contrast disparities.

With both models, we imagine a process where the generalized difference in contrast feeds into the cyclopean locus. Hence, a contrast disparity can cancel a geometric disparity. Further, the locus has a time constant giving a critical frequency of approximately 5 Hz. What distinguishes the two models is the nature of that input. The generalized difference model feeds contrast disparity into the cyclopean locus with a time constant that gives a critical frequency of about 1.3 Hz. With the gated model, however, the contrast disparity feeds into the cyclopean locus with a small time constant, giving a critical frequency in excess of 3 Hz. This input is gated by a process with a large time constant and thereby constricting input when the frequency of the stimulus reaches about 1.3 Hz. Consequently, the gated model enables the discrimination of perceived rotations induced by sine-wave temporal contrast disparity modulations from those induced by square-wave modulations at frequencies of about 1 Hz while no perceived rotation occurs at frequencies above about 1.3 Hz.

We found no systematic differences among the contrast time constants or perceived horizontal size ratio standard deviations for the fits across contrast modulation type or amplitude with the depth response. There were differences between subjects for both sets of parameters. Hence, given that the psychometric functions fit the data quite well (see Figs. 2–4), just two parameters, τ and σ_ε, can describe the six psychometric functions for a depth response measured for three amplitudes of sine-wave contrast modulations of experiment one and three amplitudes of square-wave contrast modulations of experiment two, for each subject (Table 1). One additional parameter for each subject, the perceived horizontal size ratio for motion-in-depth, allows for a description of the three psychometric functions for a motion-in-depth response. Of course, these fits are conditional upon fitting the geometric disparity data for each subject from experiment three, using two parameters, τ_{cyc} and σ_ε. A simple generalized difference model provides a succinct description of the dynamic aspects of the Venetian blind effect with respect to critical frequencies, with the gated model accounting for the discriminability between perceived rotation due to sine-wave temporal contrast disparity modulation and that due to square-wave modulation.

Critical frequencies for geometric modulations from experiment three were considerably higher than those for contrast modula-

Table 1
Estimated parameters.

Subject	τ_{cyc} Geometric (ms)	σ_{ε} Geometric (Hz)	τ Contrast (ms)	σ_{ε} Contrast (Hz)
JJD	579	0.0202	462	0.0078
WWS	403	0.1050	673	0.0275
RSH	869	0.0196	297	0.0119

Table 2
Critical frequencies.

Subject	Geometric depth (Hz)	Contrast depth (Hz)	Sine-wave motion-in-depth (Hz)
JJD	5.37	1.35	1.19
WWS	5.50	1.36	1.14
RSH	3.61	1.32	1.08

tions from experiments one and two (Fig. 7, and Table 2). Consistent with the work of Filley et al. (2011) and Hetley and Stine (2011), these results provide strong support for the notion that the physiology underlying the Venetian blind effect at moderate contrasts differs from that underlying geometric-disparity based stereopsis. The proximity of the motion-in-depth critical frequencies to the depth critical frequencies may suggest a gating mechanism.

The model that we propose seems parsimonious in the sense that a single depth locus is assumed (psychophysical linking hypothesis; Teller, 1984), based on the cancellation of a geometric disparity by a contrast disparity (Hetley & Stine, 2011; as well as cancellation by a luminance disparity, Cibis & Haber, 1951; Hetley & Stine, 2011). The output from that locus is assumed to be independent of disparity type. However, it is conceivable that two separate loci respond to depth, one from geometric disparity and one from contrast disparity, and that they reciprocally inhibit one another, enabling mutual cancellation. The contrast disparity locus might reduce its response when confronted with a rapidly varying contrast (through a gating mechanism) or, as suggested by a reviewer, a later cue combination locus might discount the contrast disparity response due to its fluctuation being deemed as less trustworthy, leaving the geometric disparity mechanism free to respond.

Another alternative model, also suggested by a reviewer, might be imagined that is a neural analogue to irradiation. In response to a dichoptic pair of square-wave gratings that are geometrically identical but with a non-zero contrast disparity, one could posit the response of two monocular channels representing the bars of the grating such that the edges of each bar in the representations are shifted toward the dark region by an amount that is positively related to the contrast across those edges. If these representations are then "fused," the individual bars should appear rotated. Our results would suggest that output from these representations into stereopsis must be gated in order to account for the low critical frequency and one's ability to discriminate perceived rotation as a function of sine-wave contrast disparity modulations from square-wave contrast disparity modulations. These channels would have to feed into stereopsis in order to account for the canceling of perceived rotation as a function of contrast disparities by geometric disparities (Hetley & Stine, 2011), be monocular in order to account for the lack of a Venetian blind effect with random-dot stereograms (Filley et al., 2011), and, finally, they would have to be distinct from representations supporting perceptions due to irradiation (e.g., the shifted-chessboard illusion; Westheimer, 2007) since the latter does exhibit spatial frequency effects (Bex & Edgar, 1996; Mather & Morgan, 1986; Morgan et al., 1984) while the former does not (Filley et al., 2011).[6] Such a model could be devised that would account for all of our data. The gated generalized-difference model seems considerably more parsimonious.

In all of these cases, one might interpret the gating mechanism as an implementation of a flat *a priori* when confronted with rapidly-changing contrast disparities. Our data cannot discriminate among these possibilities, and there are certainly many other models that would be consistent with our results.

8. General discussion

Critical frequencies to perceive depth through geometric disparity modulations are roughly 3.5 times those to perceive depth induced by contrast disparity modulations, the Venetian blind effect. As might be expected, sine-wave and square-wave contrast disparity modulations yield the same critical frequencies. Most unexpectedly, critical frequencies to perceive depth through contrast disparity modulations are only 1.2 times those to perceive motion-in-depth through sine-wave contrast disparity modulations.

That the critical frequencies for contrast modulation are much lower than those for geometric modulation argues strongly against irradiation theories, where the optics of the eye with, perhaps, an early compressive non-linearity in response, creates a perceived retinal disparity. Since there is compelling evidence that irradiation is followed by some neural processing that alters the appearance of the stimulus from work with the shifted-chessboard pattern (Westheimer, 2007), one might be tempted to argue that this neural processing is slow, thereby accounting for the low critical frequencies measured in experiments one and two. Briefly, Westheimer (2007) argues that if irradiation alone were responsible for the apparent size of the squares in the pattern, then the edges of each square should appear blurry and the corners rounded. As both appear sharp, there is clearly neural processing involved. However, given that the perceived edge placement is due to irradiation, perceived rotation would share properties with geometry based stereopsis, with critical frequencies in the range of 5 Hz and the expected spatial frequency effects. If the Venetian blind effect is caused by irradiation and neural processing is slow, the edges and corners would appear blurry if presented at, say, 3 Hz, though the perceived rotation should be easily visible.

Rather, it would seem that distinct neural channels are involved in the Venetian blind effect at moderate contrasts. Further, some sort of gating mechanism may be involved in the perception of rotation as a result of contrast disparities. Whether or not average luminance disparities, which certainly engender perceived rotation (Cibis & Haber, 1951; Filley et al., 2011), show results similar to contrast disparities is open.

It is well known that cortical processing associated with stereopsis is heavily multichannel and widely distributed, involving both the dorsal and ventral visual processing streams (see Parker, 2007, for a nice review of this literature). It is becoming increasingly clear that the pre-cortical processing that supports stereopsis involves multiple channels. In addition to what we have called monocular local edge channels, our results suggest the possible existence of monocular contrast channels, which may or may not coincide with average luminance-based channels (Filley et al.,

[6] Low-pass neural filtering followed by a compressive non-linearity would generate an edge shift. However, that combination implies an effect of stimulus blur width on perceived edge location, and thus perceived rotation with a contrast disparity (Bex & Edgar, 1996; Filley et al., 2011, Appendix D; Mather & Morgan, 1986; Morgan et al., 1984), which has not been observed (Filley et al., 2011, experiments two and three).

2011; Hetley & Stine, 2011), that feed into the cyclopean locus. Other possibilities include, perhaps, motion channels to support motion-in-depth based on motion disparities (Nefs, O'Hare, & Harris, 2010) and channels supporting contrast summation (e.g., Baker, Meese, & Georgeson, 2007; Hetley & Stine, 2011; Meese, Georgeson, & Baker, 2006) that seem to survive in the face of amblyopia (Baker et al., 2007).

Acknowledgments

We would like to acknowledge our subjects, RSH, JRH, PCN and ALC, for their extraordinary efforts and to thank Ken Fuld, Brett Gibson, Andrew Leber, John Sparrow, Colin Ware, two anonymous reviewers, and the editor Michael Landy for their helpful suggestions.

Much of the work reported was conducted in partial fulfillment for the Master of Arts and Doctor of Philosophy degrees by Dobias at the University of New Hampshire.

Stine was a Visiting Scholar at St. Edmund's College, University of Cambridge, during a sabbatical leave from the University of New Hampshire where some of this work was conducted. Support in the form of both a Faculty Scholars Program Fellowship and a College of Liberal Arts sabbatical from the University of New Hampshire is gratefully acknowledged.

Appendix A. The generalized difference model

A.1. Introduction

As mentioned previously, the dynamic model is a straightforward generalization of the model developed by Hetley and Stine (2011) along three paths. One of those paths was of the notion of a difference between the response to contrast from the two eyes in order to account for the greater range of contrasts used in the present experiments.

A.2. Generalized differences

Hetley and Stine (2011) developed a difference model of perceived rotation as a function of contrast and luminance disparities. Perceived horizontal size ratio was described as a difference between the neural contrast responses of the two eyes to rectangular-wave gratings. Each eye's neural response to contrast was described using the Naka-Rushton equation (Naka & Rushton, 1966, where $n = 1$ and $M = 0$),

$$R(C) = \frac{R_{max}C^n}{C^n + \sigma_{50}^n} + M, \tag{A1}$$

where R_{max} is the maximum response rate for the cell, C is the contrast of the rectangular-wave grating, σ_{50} is the semi-saturation constant, or that contrast that engenders a response for the cell that is half R_{max}, M is the resting response rate of the cell, and n is a constant. Perceived horizontal size ratio was described as

$$PercHSR(C_l, C_r) = gain_{eye}(R(C_l - shift) - R(C_r - shift)) + 1, \tag{A2}$$

where $gain_{eye}$ controls the gain for the input from the inter-ocular difference in neural response to contrast between the two eyes and varies depending on which eye views the higher-contrast grating, C_l and C_r are the contrasts of the gratings viewed by the left and right eyes, respectively, $R(C_{eye})$ is defined by Eq. (A1), and *shift* provides an offset along the domain of the function. When $R(C_l - shift) = R(C_r - shift)$ then $PercHSR(C_l,C_r) = 1$, so the individual bars of the grating appear to lie in the fronto-parallel plane.

Hetley and Stine (2011) measured the contrast disparity required to cancel geometric horizontal size ratios ranging from approximately 0.85 to 1.15. Over this narrow range of values, the required contrast disparities were (i) monotonically related to the horizontal size ratio and (ii) were essentially symmetric about zero, yielding perceived horizontal size ratios that were symmetric about one, as described by Eq. (2). In our studies we reached contrast disparities that not only saturated the perceived rotation, or horizontal size ratio, response, but reduced that response. Effectively, as the contrast of a grating presented to one eye becomes very much greater than that presented to the other eye, only the higher contrast grating remains visible. Hence, perceived rotation vanishes. For our range of contrast disparities, perceived horizontal size ratio is non-monotonically related to contrast disparity. Further, given that the range of horizontal size ratios is from one to zero for rotation in one direction and one to infinity for rotation in the other direction, one would expect that the ultimate range of perceived horizontal size ratios would be asymmetric about unity. To address these two issues, a generalized-difference model was developed.

The difference model of Hetley and Stine (2011) essentially describes the input of contrast to perceived horizontal size ratio as a function of contrast disparity, $R(C_l) - R(C_r)$, where R is defined by Eq. (A1). While the difference model does saturate in response, due to the saturation of response in Eq. (A1), it is monotonic with a value of zero only when $R(C_l) = R(C_r)$. Our generalized difference will be of the form

$(R(C_l) - R(C_r))\,(R(C_l) - M)(R(C_r) - M)$. The generalized difference model is non-monotonic, with a value of zero when either $R(C_l) = R(C_r)$, $R(C_l) = M$, or $R(C_r) = M$. The model exhibits the property that, as the contrast of a grating presented to one eye approaches zero, only the higher contrast grating remains visible.

Eq. (A2), from Hetley and Stine (2011), describes perceived horizontal size ratio as a difference function of the neural response to contrast. For the dynamic generalized-difference model, we describe the shift in the perceived location of each edge in a rectangular-wave grating as a function of contrast disparity. We then use the perceived edge shift to calculate a perceived horizontal size ratio, thereby generating the asymmetry in perceived horizontal size ratio as a function of contrast disparity.

Appendix B. Fitting the dynamic generalized difference model

The generalized difference model was fit to the psychometric functions measured in experiments one through three. Using the parameters from that fit, the gated generalized difference model was then to predict perceived rotation for the some of the data from experiments one and two.

In order to map from Eq. (4) to probability of seeing depth, it was assumed that a perceived horizontal size ratio of 1.05 or greater would engender a depth response. This value corresponds to a small perceived rotation from Hetley and Stine (2011). Using Eq. (4), a predicted perceived horizontal size ratio was generated for a given stimulus configuration. A Laplace cumulative distribution with a mean of 1.05 and a particular standard deviation, σ_ε, was used to generate the probability of seeing depth. An intensity difference model leads naturally to a Laplace distribution (Filley et al., 2011). We have also found that the Laplace, which is leptokurtic, tends to fit our data slightly better than the Gaussian or Weibull.

Again following Hetley and Stine (2011), the parameters for the Naka-Rushton equation (Eq. (A1)) were set to the values used by Sclar, Maunsell, and Lennie (1990) to describe V1 cells in *M. fascicularis*, giving $R_{max} = 27.4$ imp/s, $M = 8.22$ imp/s, and $n = 2.4$. From Hetley and Stine (Submitted), $\sigma_{50} = 0.15$. Finally, $gain = 1.496 \times 10^{-5}$ deg/imp/s, which is the value used by Hetley and Stine (2011) scaled by the ratio of the maximum of the difference

equation to that of the generalized difference equation. Hence, all of these parameter values were defined independently of our data.

The remaining three parameters, τ_{cyc}, τ, and σ_{ε}, were fit sequentially to data from each subject. First, for a given subject, the least-squares values for τ_{cyc} and σ_{ε} were found to predict that subject's probability of seeing depth from geometric modulations as measured in experiment three. During this step $\tau = \tau_{cyc}/100$, thereby effectively giving a value for τ_{cyc} that reflects the time limits imposed at the cyclopean locus. The psychometric functions plotted in Fig. 4 for the geometric disparities are the result of these fits. Next, the least-squares fits of psychometric functions was calculated for the three largest amplitudes from the sine-wave and square-wave contrast disparity modulation experiments using τ and σ_{ε} while using τ_{cyc} from that subject's geometric fit. Recall that at least one subject failed to perceive depth for each of the two smaller amplitudes. Hence, two parameters, τ_{cyc} and σ_{ε}, were used to fit the geometric data from each subject and then two more parameters, τ and σ_{ε} were used to fit each of the three largest amplitudes for the sine-wave and square-wave contrast modulation psychometric functions. For each subject, 14 parameters were used to fit the seven psychometric functions plotted in Figs. 2–4.

The psychometric functions for the motion-in-depth response to the sine-wave contrast modulations of experiment one were fit using the parameters from the depth response while allowing the threshold perceived horizontal size ratio to deviate from 1.05. Hence, conditional upon the fit of the three psychometric functions to the depth response data from experiment one, three perceived horizontal size ratio parameters were used to fit the three psychometric functions to the motion-in-depth response data across the three largest contrast modulation amplitudes for each subject.

All of the modeling was programed using *Mathematica 7*. For a given psychometric function, either with geometric modulations or contrast modulations that could be sine-wave or square-wave in form and of three possible amplitudes, we generated predictions for the various temporal frequencies (step = 1.0 Hz) using a range of time constants and Laplace standard deviations over a 10 s time interval in 1 ms steps. Predictions from system of Eq. (1) were generated using the *Mathematica* routine *NDSolve* with *MaxStepFraction* = 0.001 and *MaxSteps* = 100,000, otherwise default options were used. From system (1), the maximum of the solution $g(t)$, symbolically represented as Eq. (3), was located using the routine *NMaximize* restricted to the interval 5 s to 9 s. The resulting maximum horizontal size ratio was calculated using Eq. (4). We then used the routine *CDF* with *LaplaceDistribution* and a mean of 1.05 to generate the predicted probability of seeing depth. Using the routine *NMinimize*, we then found the time constant and standard deviation for the Laplace distribution that minimized the sum of squared errors between the empirical relative frequencies of seeing depth and those predicted by the model from the interpolation for each subject.

To generate predictions for perceived rotation as a function of both a square-wave contrast disparity modulation and a sine-wave contrast disparity modulation with an amplitude of 0.6 and a frequency of 1.0 Hz (Fig. 8), we generated the prediction of the generalized difference model using perceived edge shift from Eq. (3) and the resulting perceived horizontal size ratio change from Eq. (4). For the gated generalized difference model we generated perceived edge shift from Eq. (5), with parameters *gain* = 0.132 s of retinal arc and critical frequency ω = 1.35 Hz, and the resulting perceived horizontal size ratio change from Eq. (4). Perceived rotation was then calculated from perceived horizontal size ratio using Eq. (B1)

$$s(t) = -Arctan\left(\frac{2d(hsr(t) - vsr^2)}{ipCos(\gamma)(hsr(t) + vsr^2)} + Tan(\gamma)\right), \tag{B1}$$

where d = 1.58 m is the distance from the pupil to the screen surface, $hsr(t)$ is the perceived horizontal size ratio (Eq. (4) as a function of either $g(t)$, upper panel, or $p(t)$, lower panel), vsr = 1 is the vertical size ratio, ip = 0.06 m is the inter-ocular distance, and γ = 0 is the azimuth of gaze (Backus et al., 1999, Eq. (A5); note that this equation was developed from geometric considerations rather than perceptual ones).

Appendix C. Analyses of variance

C.1. Introduction

Again, just three parameters, the geometric disparity time constant τ_{cyc}, the contrast disparity time constant, τ, and the perceived horizontal size ratio standard deviation, σ_{ε}, should suffice in order to describe the three psychometric functions defined by the depth response to contrast disparity modulations for each of the three subjects and a threshold shift should be sufficient to encompass the psychometric functions defined by the motion-in-depth response for each subject.

Three analyses of variance (ANOVA) were conducted on the parameter estimates. Using the contrast disparity time constant, τ, and the perceived horizontal size ratio standard deviation, σ_{ε}, as dependent variables, two ANOVAs were conducted in the context of a repeated-measures, randomized-block factorial design using two within-subject independent variables, contrast modulation type with two levels (square-wave contrast modulation with a depth response and sine-wave contrast modulation with a depth response) and contrast disparity amplitude with three levels (0.6, 0.8, and 1.0), giving two-by-three designs (RBF-23; Kirk, 1995, chap. 10.5–10.9). None of the main effect or interactions should be significant if the model can describe each subject's data with three parameters. A third ANOVA, using a one-way repeated measures design, was conducted on the perceived horizontal size ratios threshold parameters from the motion-in-depth response psychophysical functions across the three contrast disparity modulation amplitudes (0.6, 0.8, 1.0; RB-3, Kirk 1995, chap. 7).

For the randomized-block factorial ANOVA that was conducted on the logarithm of the critical frequencies, we used two within-subject independent variables, contrast modulation/response type with three levels (square-wave contrast modulation with a depth response, sine-wave contrast modulation with a depth response, and sine-wave contrast modulation with a motion-in-depth response) and contrast disparity amplitude with three levels (0.6, 0.8, and 1.0), giving a three-by-three design (RBF-33; Kirk, 1995, chap. 10.5–10.9).

Since the four ANOVAs were applied to correlated data, a Holm's sequentially rejective Šidák procedure was used to hold the family-wise type I error rate to $\alpha_{familywise}$ = 0.05 (Holm, 1979; Kirk, 1995, pp. 142–144). For the factorial designs, tests of the two main effects, the interaction, and subjects are mutually orthogonal. Therefore, the Holm's procedure was applied across the three tests for contrast disparity modulation type/response effects, four tests for contrast disparity modulation amplitude effects, and four tests for differences among the three subjects. Data from JRH was not included in this analysis since she only viewed the 0.6 amplitude condition.

C.2. Checking assumptions

Normality was checked by plotting the dependent variables on normal-probability axes. Additivity assumptions were checked using tests of subject by independent variable interactions for the factorial designs and Tukey's tests for non-additivity (Kirk, 1995; Tukey, 1949, chap. 7.3) for all four designs, with $\alpha_{family-}$

$_{wise}$ = 0.10 (Kirk, 1995, p. 103, p. 269). When appropriate, the degrees of freedom for an analysis was adjusted using the Geisser–Greenhouse $\hat{\varepsilon}$ to control for the deviation of the given variance–covariance matrix from sphericity (Collier et al., 1967; Geisser & Greenhouse, 1958; Kirk, 1995, pp. 274–282).

Model time constants τ. The contrast time constants appeared normally distributed though the variance–covariance matrix appeared non-spherical ($\hat{\varepsilon} = 0.310$). An additive model appeared appropriate (subjects by contrast modulation type: $F(2,4) = 2.12$, $p = 0.237$, $MSRES = 2763$ Holm's step one $\alpha_{test} = 0.0345$; subjects by contrast disparity modulation amplitude: $F(4,4) = 2.40$, $p = 0.208$, $MSRES = 2763$, Holm's step one $\alpha_{test} = 0.0345$; Tukey's test of non-additivity: $F(1,9) = 0.120$, $p = 0.737$, $MSRES = 5401$; Holm's step two $\alpha_{test} = 0.0345$).

Perceived horizontal size ratio standard deviation $\sigma_{\hat{\varepsilon}}$. The standard deviations fell into two clusters in the normal probability plot, and so appeared non-normal though without outliers. The variance–covariance matrix appeared non-spherical ($\hat{\varepsilon} = 0.319$). While subjects did not interact with contrast modulation type or magnitude (subjects by contrast modulation type: $F(2,4) = 1.154$, $p = 0.0588$, $MSRES = 0.0000329$, Holm's step one $\alpha_{test} = 0.0345$; subjects by contrast modulation amplitude: $F(4,4) = 0.646$, $p = 0.659$, $MSRES = 0.0000329$, Holm's step one $\alpha_{test} = 0.0345$), Tukey's test of non-additivity was significant ($F(1,9) = 16.4$, $p = 0.00290$, $MSRES = 0.0000247$; Holm's step one $\alpha_{test} = 0.0260$), suggesting that we may have some loss of power (Kirk, 1995, chap. 7.3).

Perceived horizontal size ratio thresholds for motion-in-depth. The parameters representing the threshold horizontal size ratio to see motion in depth exhibited a small amount of positive skew in the normal probability plot. The variance–covariance matrix appeared non-spherical ($\hat{\varepsilon} = 0.542$). There was no evidence of a violation of additivity (Tukey's test of non-additivity: $F(1,3) = 0.210$, $p = 0.678$, Holm's step two $\alpha_{test} = 0.0345$).

Critical frequencies. Log critical frequencies appeared to deviate marginally from a normally with some positive skew. The variance–covariance matrix appeared non-spherical ($\hat{\varepsilon} = 0.383$). An additive model appeared appropriate (subjects by contrast modulation/response type: $F(4,8) = 2.58$, $p = 0.118$, $MSRES = 0.00118$, Holm's step one $\alpha_{test} = 0.0345$; subjects by contrast modulation amplitude: $F(4,8) = 3.96$, $p = 0.0464$, $MSRES = 0.00118$, Holm's step one $\alpha_{test} = 0.0345$; Tukey's test of non-additivity: $F(1,23) = 0.746$, $p = 0.401$; Holm's step two $\alpha_{test} = 0.0345$).[7]

C.3. Results

Model time constants τ. Time constants differed across subjects ($F(2,10) = 45.6$, $p = 9.44 \times 10^{-6}$, $\rho_I = 0.901$, $MSRES = 4926$, Holm's step one $\alpha_{test} = 0.0127$). Time constants did not differ across contrast disparity modulation type, amplitude, or their combinations (Type: $F(1,10) = 3.70$, $\hat{\varepsilon}$ adjusted $p = 0.122$, Holm's step one $\alpha_{test} = 0.01695$; Amplitude: $F(2,10) = 5.51$, $\hat{\varepsilon}$ adjusted $p = 0.097$, Holm's step one $\alpha_{test} = 0.0127$; Type × Amplitude: $F(2,10) = 1.73$, $\hat{\varepsilon}$ adjusted $p = 0.245$, Holm's step one $\alpha_{test} = 0.0127$ $MSRES = 4926$ for all three tests), as expected.

Perceived horizontal size ratio standard deviation $\sigma_{\hat{\varepsilon}}$. The standard deviations differed among subjects ($F(2,10) = 9.45$, $p = 0.00495$, $\rho_I = 0.654$, $MSRES = 0.0000627$, Holm's step one $\alpha_{test} = 0.0127$). Standard deviations did not differ across contrast modulation type, amplitude, or their combinations (Type: $F(1,10) = 3.78$, $\hat{\varepsilon}$ adjusted $p = 0.119$, Holm's step one $\alpha_{test} = 0.01695$; Amplitude: $F(2,10) = 0.809$, $\hat{\varepsilon}$ adjusted $p = 0.368$, Holm's step one $\alpha_{test} = 0.0127$; Type × Amplitude: $F(2,10) = 0.130$, $\hat{\varepsilon}$ adjusted $p = 0.626$, Holm's step one $\alpha_{test} = 0.0127$, $MSRES = 0.0000627$ for all three tests), as expected.

Perceived horizontal size ratio thresholds for motion-in-depth. The threshold parameters did not differ among subjects ($F(2,4) = 1.35$, $p = 0.357$, Holm's step three $\alpha_{test} = 0.0513$) or across contrast modulation amplitudes ($F(2,4) = 0.967$, $p = 0.432$, Holm's step one $\alpha_{test} = 0.0127$). Again, one parameter suffices across contrast modulation amplitudes.

Critical frequencies. Log critical frequencies did not differ across subjects ($F(2,16) = 1.84$, $p = 0.190$, $MSRES = 0.00251$, Holm's step four $\alpha_{test} = 0.05$). Log critical frequencies did vary across contrast modulation type/response ($F(2,16) = 35.6$, $\hat{\varepsilon}$ adjusted $p = 0.00126$, partial $\hat{\omega}^2 = 0.719$, $MSRES = 0.002511$, Holm's step one $\alpha_{test} = 0.0170$). The effect of contrast modulation amplitude might be viewed as marginal ($F(2,16) = 9.73$, $\hat{\varepsilon}$ adjusted $p = 0.0236$, partial $\hat{\omega}^2 = 0.393$, Holm's step one $\alpha_{test} = 0.0127$; $MSRES = 0.002511$), given that $0.0127 < p < 0.05$. No evidence for a contrast modulation type/response × contrast modulation amplitude was found ($F(4,16) = 1.13$, $\hat{\varepsilon}$ adjusted $p = 0.363$, $MSRES = 0.002511$, Holm's step one $\alpha_{test} = 0.0170$).

A posteriori multiple comparisons were conducted across both contrast modulation type/response and contrast modulation amplitude using Scheffé S tests with local error terms (Kirk, 1995, pp. 154–155 and 283–285; Scheffé, 1953). The log critical frequency averaged across depth responses for both square-wave and sine-wave modulations differed from log critical frequency averaged across sine-wave modulations for a motion-in-depth response ($F(1,6) = 11.6$, Scheffé S test $p = 0.0127$, partial $\hat{\omega}^2 = 0.541$, $MSRES_{\psi} = 0.0872$). We also compared log critical frequency averaged across square-wave contrast modulations with a depth response to log critical frequency averaged across sine-wave contrast modulations with a depth response, and linear and quadratic trends in log critical frequency across contrast modulation amplitudes averaged over contrast modulation type/response, none of which were significant (square-wave vs. sine-wave with depth response: $F(1,6) = 4.07$, Scheffé S test $p = 0.163$, $MSRES_{\psi} = 0.0113$; linear trend across amplitudes: $F(1,6) = 5.87$, Scheffé S test $p = 0.0820$, $MSRES_{\psi} = 0.0366$; quadratic trend across amplitudes: $F(1,6) = 0.934$, Scheffé S test $p = 0.635$, $MSRES_{\psi} = 0.00184$).

[7] Note that the subjects by contrast modulation amplitude may be considered marginal (i.e., significant at $\alpha_{test} = 0.05$ level though not significant with $\alpha_{family\text{-}wise} = 0.05$). When the subjects by contrast modulation type/response is pooled with the error term, the subjects by contrast modulation amplitude becomes clearly non-significant ($F(4,12) = 2.56$, $p = 0.0900$, $MSRES = 0.00180$, Holm's step one $\alpha_{test} = 0.0345$; Kirk, 1995, pp. 408–411).

References

Agresti, A., & Coull, B. A. (1998). Approximate is better than "exact" for interval estimation of binomial proportions. *The American Statistician, 52*, 119–126.

Backus, B. T., Banks, M. S., van Ee, R., & Crowell, J. A. (1999). Horizontal and vertical disparity, eye position, and stereoscopic slant perception. *Vision Research, 33*, 1143–1170.

Baker, D. H., Meese, T. S., & Georgeson, M. A. (2007). Binocular interaction: Contrast matching and contrast discrimination are predicted by the same model. *Spatial Vision, 20*, 397–413.

Baker, D. H., Meese, T. S., Mansouri, B., & Hess, R. F. (2007). Binocular summation of contrast remains intact in strabismic amblyopia. *Investigative Ophthalmology and Visual Science, 48*, 5332–5338.

von Békésy, G. (1970). Apparent image rotation in stereoscopic vision: The unbalance of the pupils. *Perception and Psychophysics, 8*, 343–347.

Beverley, K. I., & Regan, D. (1973a). Evidence for the existence of neural mechanisms selectively sensitive to the direction of movement in space. *Journal of Physiology, 235*, 17–29.

Beverley, K. I., & Regan, D. (1973b). Selective adaptation in stereoscopic depth perception. *Journal of Physiology, 232*. 40–41P.

Beverley, K. I., & Regan, D. (1974a). Temporal integration of disparity information in stereoscopic perception. *Experimental Brain Research, 19*, 228–232.

Beverley, K. I., & Regan, D. (1974b). Visual sensitivity to disparity pulses. *Vision Research, 14*, 357–361.

Bex, P. J., & Edgar, G. K. (1996). Shifts in the perceived location of a blurred edge increase with contrast. *Perception and Psychophysics, 58*, 31–33.

Blake, R., & Cormack, R. H. (1979). Does contrast disparity alone generate stereopsis? *Vision Research, 19*, 913–915.

Bridgeman, G., Hendry, D., & Stark, L. (1975). Failure to detect displacement of visual world during saccadic eye movements. *Vision Research, 15*, 719–722.
Chen, Y., & Qian, N. (2004). A coarse-to-fine disparity energy model with both phase-shift and position shift receptive field mechanisms. *Neural Computation, 16*, 1545–1577.
Cibis, P. A., & Haber, H. (1951). Anisopia and perception of space. *Journal of the Optical Society of America, 41*, 676–683.
Collier, R. O., Jr., Baker, F. B., Mandeville, G. K., & Hayes, T. F. (1967). Estimates of test size for several test procedures based on conventional variance ratios in the repeated measures design. *Psychometrika, 32*, 339–353.
Filley, E. T., Khutoryansky, N., Dobias, J. J., & Stine, W. W. (2011). An investigation of the Venetian blind effect. *Seeing and Perceiving, 24*, 241–292.
Fiorentini, A., & Maffei, L. (1971). Binocular depth perception without geometrical cues. *Vision Research, 11*, 1299–1305.
Geisser, S., & Greenhouse, S. W. (1958). An extension of Box's results on the use of the F distribution in multivariate analysis. *Annals of Mathematical Statistics, 29*, 885–891.
Hetley, R. S., & Stine, W. W. (2011). Partitioning contrast or luminance disparity into perceived intensity and rotation. *Seeing and Perceiving, 24*, 315–350.
Holm, S. (1979). A simple sequentially rejective multiple test procedure. *Scandinavian Journal of Statistics, 6*, 65–70.
Howard, I. P., & Rogers, B. J. (1995). *Binocular vision and stereopsis*. New York, NY: Oxford University Press.
Ikeda, M. (1986). Temporal impulse response. *Vision Research, 26*(9), 1431–1440.
Kelly, D. H. (1979). Motion and vision. II. Stabilized spatio-temporal threshold surface. *Journal of the Optical Society of America, 69*, 1340–1349.
Kirk, R. E. (1995). *Experimental design: Procedures for the behavioral sciences* (3rd ed.). Pacific Grove, CA: Brooks/Cole.
Loftus, G. R., & Masson, M. E. J. (1994). Using confidence intervals in within-subject designs. *Psychonomic Bulletin and Review, 1*, 476–490.
Losada, M. A., Navarro, R., & Santamaría, J. (1993). Relative contributions of optical and neural limitations to human contrast sensitivity at different luminance levels. *Vision Research, 33*, 2321–2336.
Mansfield, J. S., & Legge, G. E. (1996). The binocular computation of visual direction. *Vision Research, 36*, 27–41.
Mather, G., & Morgan, M. J. (1986). Irradiation: Implications for theories of edge localization. *Vision Research, 26*, 1007–1015.
Meese, T. S., Georgeson, M. A., & Baker, D. H. (2006). Binocular contrast vision at and above threshold. *Journal of Vision, 6*, 1224–1243.
Michelson, A. A. (1927). *Studies in optics*. Chicago: University of Chicago Press, Ltd. (1962 reprint).
Morgan, M. J., Mather, G., Moulden, B., & Watt, R. J. (1984). Intensity response nonlinearities and the theory of edge localization. *Vision Research, 24*, 713–719.
Münster, C. (1941). Ueber den Einfluss von Helligkeitsunterschieden in beiden Augen auf die stereoskipische Wahrnehmung. *Zeitschrift für Sinnesphysiologie, 69*, 245–260.
Naka, K. I., & Rushton, W. A. H. (1966). S-potentials from luminosity units in the retina of fish (Cyprinidae). *Journal of Physiology, 185*, 587–599.
Nefs, H. T., O'Hare, L., & Harris, J. M. (2010). Two independent mechanisms for motion-in-depth perception: Evidence from individual differences. *Frontiers in Psychology, 1*, 1–8.
Norman, M. F. (1981). Lectures on linear systems theory. *Journal of Mathematical Psychology, 23*, 1–89.
Ogle, K. N. (1962). The optical space sense. In H. Davson (Ed.). *The eye* (Vol. 4, pp. 211–417). New York: Academic Press.
Parker, A. J. (2007). Binocular depth perception and the cerebral cortex. *Nature Reviews Neuroscience, 8*, 379–391.
Regan, D., & Beverley, K. I. (1973a). Some dynamic features of depth perception. *Vision Research, 13*, 2369–2379.
Regan, D., & Beverley, K. I. (1973b). The dissociation of sideways movements from movements in depth: Psychophysics. *Vision Research, 13*, 2403–2415.
Richards, W. (1972). Response functions for sine- and square-wave modulations of disparity. *Journal of the Optical Society of America, 62*(7), 907–911.
Scheffé, H. (1953). A method for judging all contrasts in the analysis of variance. *Biometrika, 40*, 87–104.
Schor, C. M., & Wood, I. (1983). Disparity range for local atereopsis as a function of luminance spatial frequency. *Vision Research, 23*, 1649–1654.
Schor, C. M., Wood, I., & Ogawa, J. (1984). Spatial tuning of static and dynamic local stereopsis. *Vision Research, 24*, 573–578.
Sclar, G., Maunsell, J. H. R., & Lennie, P. (1990). Coding of image contrast in central visual pathways of the macaque monkey. *Vision Research, 30*, 1–10.
Teller, D. Y. (1984). Linking propositions. *Vision Research, 24*, 1233–1246.
Tukey, J. W. (1949). One degree of freedom for non-additivity. *Biometrics, 5*, 232–242.
von Helmholtz, H. (1911/1924). Helmholtz's treatise on physiological optics. In J. P. C. Southall (Ed.), *The sensations of vision* (Vol. II, Trans. from 3rd ed.). Menasha, WI: Optical Society of America.
Weiler, J. A., Maxwell, J. S., & Schor, C. M. (2007). Illusory contrast-induced shifts in binocular visual direction bias saccadic eye movements towards the perceived target position. *Journal of Vision, 7*(5), 1–18.
Westheimer, G. (2007). Irradiation, border location, and the shifted-chessboard pattern. *Perception, 36*, 483–494.
White, K. D., & Odom, J. V. (1985). Temporal integration in global stereopsis. *Perception and Psychophysics, 37*(2), 139–144.
Wilson, E. B. (1927). Probable inference, the law of succession, and statistical inference. *Journal of the American Statistical Association, 22*, 209–212.